frontiers | Frontiers in Materials

ORIGINAL RESEARCH
published: 16 May 2022
doi: 10.3389/fmats.2022.902139

Sustainable Alkali-Activated Slag Binders Based on Alternative Activators Sourced From Mineral Wool and Glass Waste

*Majda Pavlin[1], Katja König[1], Jakob König[2], Uroš Javornik[3] and Vilma Ducman[1]**

[1]Slovenian National Building and Civil Engineering Institute (ZAG Ljubljana), Ljubljana, Slovenia, [2]Jožef Stefan Insitute, Ljubljana, Slovenia, [3]Slovenian NMR Centre, National Institute of Chemistry, Ljubljana, Slovenia

In the present study, four different locally available waste glass materials (bottle glass-BG, glass wool-GW, stone wool-SW and cathode-ray tube glass-CRTG) were treated with hot concentrated potassium hydroxide (KOH) in order to obtain alternative alkali activators (AAAs). We evaluated the suitability of the solutions obtained for use as AAAs in the production of AAMs. AAMs were prepared using electric arc furnace slag and selected AAAs with a higher content of dissolved Si. We evaluated the performance of the AAMs in comparison to that of slags activated with KOH or potassium-silicate (K-silicate). The compressive strength of the AAMs prepared with KOH-based AAAs were high when Si and Al were simultaneously abundant in the AAA (9.47 MPa when using the activator sourced from the CRTG), and low with the addition of KOH alone (1.97 MPa). The AAM produced using commercial K-silicate yielded the highest compressive strength (27.7 MPa). The porosity of the KOH-based AAM was lowest when an alternative BG-based activator was used (24.1%), when it was similar to that of the AAM prepared with a K-silicate. The BG-based activator had the highest silicon content (33.1 g/L), and NMR revealed that Si was present in the form of Q^0, Q^1 and Q^2. The concentrations of toxic trace elements in the AAAs used for alkali activation of the slag were also determined, and leaching experiments were performed on the AAMs to evaluate the immobilisation potential of alkali-activated slag. In the SW AAAs the results show acceptable concentrations of trace and minor elements with respect to the regulations on waste disposal sites, while in the activators prepared from BG, CRTG and GW some elements exceeded the allowable limits (Pb, Ba, Sb, and As).

Keywords: alkali-activated materials, alternative activators, waste glass, waste mineral wool, cathode-ray tube glass, bottle glass, solubility, leaching

OPEN ACCESS

Edited by:
Isabella Lancellotti, University of Modena and Reggio Emilia, Italy

Reviewed by:
Ping Duan, China University of Geosciences Wuhan, China
Kenneth John MacKenzie, MacDiarmid Institute for Advanced Materials and Nanotechnology, New Zealand

****Correspondence:***
Vilma Ducman
vilma.ducman@zag.si

Specialty section:
This article was submitted to Structural Materials, a section of the journal Frontiers in Materials

Received: *22 March 2022*
Accepted: *26 April 2022*
Published: *16 May 2022*

Citation:
Pavlin M, König K, König J, Javornik U and Ducman V (2022) Sustainable Alkali-Activated Slag Binders Based on Alternative Activators Sourced From Mineral Wool and Glass Waste. Front. Mater. 9:902139. doi: 10.3389/fmats.2022.902139

INTRODUCTION

Generally, the global warming potential of alkali-activated materials (AAMs) is estimated to be between 45% and 80% lower than that of Ordinary Portland cement (OPC), depending on the precursor and activator used for synthesis (Habert et al., 2011; McLellan et al., 2011; Yang et al., 2013; Ouellet-Plamondon et al., 2015). Turner and Collins, however, estimated that the CO_2 footprint of alkali-activated concrete was much higher—approximately 9% lower than comparable concrete containing 100% OPC binder—due to the processes of mining and synthesis (e.g., the

highly energy-demanding process required to produce water glass), and the transport of alkali activators required for the production of AAMs (Turner and Collins, 2013). The production of commercial alkali activators accounts for about 80% of the cost of the production of AAMs. The production of a sodium silicate activator, for example, requires SiO_2 and Na_2CO_3 to be heated to temperatures of over 1,000°C. Due to the high energy and environmental cost of traditionally-produced sodium silicate (≈ 0.30 kg CO_2/kg) (Heath et al., 2014), it is necessary to develop alternative alkali activators (AAAs) from environmentally friendly residual (waste) materials. AAAs are not usually as pure as those based on commercial synthetic chemicals (Adesanya et al., 2021).

One promising and innovative approach to reducing the environmental impact of AAMs is to use different types of waste and by-products from industrial and agricultural processes that have a high content of alkali metals, alkali earth metals, and/or silicon. Potentially interesting materials with a high silica content (e.g., waste glass, waste mineral wool, biomass ashes such as rice husk ash (RHA) or sugarcane biomass ash, and silica fume) are typically combined with alkali hydroxides (NaOH, KOH), with or without the use of thermochemical methods (Adesanya et al., 2021). The dissolution of Si-rich particles therefore depends on the degree of aggregation, the surface area, and the particle shape and size (Diedrich et al., 2012; Torres-Carrasco et al., 2014; El-Naggar and El-Dessouky, 2017). To date, no standard method exists to prepare such AAAs. It is, however, generally expected that the processes of heating and stirring enhance the dissolution rate of Si, as the kinetics of chemical reactions usually increases with temperature and an external stimulus (Alnahhal et al., 2021). The scientific literature discusses several experimental processes; fusion, hydrothermal and thermochemical. In the fusion process, for example a Si-rich precursor and NaOH pellets are heated to 550°C, and then the mixture is dissolved in distilled water. The fusion process does not, however, significantly reduce the environmental impact of the prepared activator (El-Naggar and El-Dessouky, 2017). Lower temperatures, typically below 150°C, are applied in the hydrothermal process. At 80°C, for example, different studies show relatively high dissolution rates of Si from RHA (Tong et al., 2018) and waste glass (Puertas and Torres-Carrasco, 2014; Torres-Carrasco et al., 2014; Torres-Carrasco and Puertas, 2015). Temperatures of up to 450°C are used in the thermochemical process to transform the solid alkali and silica sources into reactive sodium silicate powder. Several studies have shown that the most effective temperatures for the production of sodium silicate powder are in the range between 150°C and 330°C (Vinai and Soutsos, 2019). Dissolution is a temperature-dependent process with a higher yield of dissolved Si being obtained at higher temperatures (Alnahhal et al., 2021). Due to the high activation energy of amorphous silica (Maraghechi et al., 2016), higher temperatures are required in the hydrothermal process to achieve the activation energy of Si in alkaline solutions and increase the yield of dissolved Si (Alnahhal et al., 2021).

AAAs are most commonly produced from industrial or agricultural wastes that are rich in silica and alkali cations such as potassium or sodium, e.g., rice husk ash (RHA) (Bouzón et al., 2014; Mejía et al., 2014; Geraldo et al., 2017; Tong et al., 2018), waste glass (Torres-Carrasco and Puertas, 2015; Tchakouté et al., 2016a; Vinai and Soutsos, 2019), silica fume (Živica, 2006; Rodríguez et al., 2013) and others (sugar cane straw ash (Moraes et al., 2016), olive biomass ash (Font et al., 2017; de Moraes Pinheiro et al., 2018; Alonso et al., 2019), almond shell biomass ash (Soriano et al., 2020)). AAAs derived from RHA have a silica content between 85–95 wt%, where not all silica is in the reactive form (Bouzón et al., 2014; Mejía et al., 2014; Geraldo et al., 2017; Tong et al., 2018). Tang et al. proved that an RHA-based activator is an adequate substitute for commercial sodium silicate in the production of AAMs using 60 wt% fly ash (FA) and 40 wt% ground granulated blast furnace slag (GGBFS) (Tong et al., 2018). AAAs have often been prepared using glass waste (Puertas and Torres-Carrasco, 2014; Torres-Carrasco et al., 2014; Torres-Carrasco and Puertas, 2015; König et al., 2020). The preparation of different AAAs using urban glass waste shows decreased mechanical properties in FA when the alkali activator is prepared with a higher amount of waste (25 g per 100 ml of 10 M NaOH). For comparison, using 15 g per 100 ml of 10 M NaOH, the mechanical strengths of alkali-activated FA were similar to those prepared by a commercial activator (Torres-Carrasco and Puertas, 2015). Similar findings were proved in the study by Vinai and Soutos, where alkali-activated FA/GGBFS mortars activated with AAAs based on ground glass waste showed compressive strengths close to those obtained when using commercial sodium silicate (Vinai and Soutsos, 2019). When comparing the mechanical strength of AAMs prepared using AAAs of RHA or glass waste, AAMs made using glass waste show better properties, due to the higher amounts of soluble Si (Tchakouté et al., 2016a). There has been only one publication investigating the use of mineral wool waste for the preparation of AAAs (König et al., 2020). Mineral wool, glass- (GW), and stone wool (SW) are suitable precursors as their content of amorphous phase is almost 100%, with SW containing approximately 40 wt% SiO_2 and GW 60 wt% (Pavlin et al., 2021).

Due to the higher energy incorporation and CO_2 emissions of the manufacturing process, the cost is higher and availability of potassium hydroxide (KOH) and potassium silicate (K-silicate) is lower compared to sodium products (Mendes et al., 2021). From an environmental perspective, AAMs are already clearly superior to cement-based products (Jiang et al., 2014), but with the production of AAAs, this advantage would be even more pronounced. Indeed, previous studies have confirmed that besides electricity, most of the environmental impact comes from silicates and hydroxide (Kvočka et al., 2020). And when comparing different activators, K-based activators have also been shown to increase global warming potential by 4% compared to Na-based activators; in both cases, commercial activators were used (Leonelli et al., 2022). Further progress in terms of environmental aspects could therefore be achieved by producing AAAs, which is one of the objectives of the present study. It follows that there are fewer studies available that use KOH for the preparation of AAAs. Villaquirán-Caicedo reports on AAAs prepared by adding silica fume to 9.3 M KOH and used to activate metakaolin. The metakaolin-based AAMs showed

better mechanical properties when 50% of the commercial activator was replaced with the alternative, while mechanical strength decreased with 100% replacement (Villaquirán-Caicedo, 2019). In another study, 5 M and 8 M NaOH and KOH solutions were utilised to dissolve glass waste at 65°C for 2 hours. The compressive strength of the AAMs activated by NaOH were higher than those activated by KOH (Bagheri and Moukannaa, 2021). On the contrary, AAMs prepared by KOH-based AAAs had a higher compressive strength in the study by Santa et al. (Boca Santa et al., 2017).

The goal of the present research was to treat four different locally available waste glass materials (bottle glass-BG, glass wool-GW, stone wool-SW, and cathode-ray tube glass-CRTG) with KOH, and to evaluate the suitability of the solutions obtained for use as AAAs in the preparation of AAMs. AAMs were prepared with slag and selected AAAs with a higher amount of dissolved Si, and their performance was evaluated in comparison to slag activated with KOH or K-silicate. Compared to our previous results with respect to materials based on NaOH (König et al., 2020), adding AAAs based on KOH resulted in the alkali-activated binders having a higher mechanical strength. Moreover, the concentrations of toxic trace elements in AAAs used for alkali activation of the slag were determined and leaching experiments were performed on the AAMs in order to evaluate the immobilization potential of the alkali-activated slag using AAAs.

EXPERIMENTAL

Raw Materials for the Preparation of Alternative Activators and Alkali-Activated Binders

Various types of waste material obtained from a waste separation site were used for the preparation of alkali activators; glass wool (GW), stone wool (SW), bottle glass (BG), and cathode-ray tube glass (CRTG). Both types of mineral wool were milled for 2 hours in a concrete mixer using stainless steel balls, homogenised and dried at 105°C for 24 h in a drying oven, and then sieved to a particle size of below 63 μm. The bottle glass and cathode-ray tube glass were milled, homogenised and sieved to a particle size of below 90 μm.

Electric arc furnace slag (EAFS) from the metallurgical industry in Slovenia was used as a precursor for the preparation of alkali-activated binders. The slag was milled, homogenised and sieved to a particle size of below 90 μm.

Characterisation of the Raw Materials

The chemical composition of the raw materials was determined by Sequential X-Ray Fluorescence (XRF) Spectrometer (ARL PERFORM′X, Thermo Fisher Scientific Inc., USA) using UniQuant software. Before measurement, powder samples were heated at 950°C and then fused beads were prepared at 1,050°C—1,100°C using commercially available flux composed of 50% lithium tetraborate and 50% lithium metaborate (FX-X50-2, Fluxana GmbH & Co. KG, Germany). The mass ratio of powder to flux was 1:10.

Nitrogen sorption (ASAP 2020, Micromeritics, Norcross, USA), at a temperature of 77K and relative pressure range between 0.05 and 0.3, was used to determine the specific surface area of the powders. Before each measurement, the powders were heated to 70°C–105°C for at least 3 h and degassed to 0.133 Pa (Flowprep equipment, Micromeritics, Norcross, GA, USA). The specific surface area was calculated using the Brunauer–Emmett–Teller (BET) method.

Particle size distribution was determined by laser granulometry (Microtrac MRB Sync, part of Verder Scientific). The chemical composition, BET surface area and particle size (d10, d50, d90) of the raw materials used for the preparation of AAAs and the precursor used for alkali activation are shown in the **Supplementary Table S1** and **Supplementary Figure S1**. The initial waste materials for the preparation of AAAs contained different amounts of SiO_2. BG contained 72.4 wt% SiO_2, GW 65.4 wt% SiO_2, CRTG 58.5 wt% SiO_2, while the SW contained the lowest amount of SiO_2 (43.6 wt%). Stone wool had the highest amount of Al_2O_3 (16.1 wt%), while the other waste glasses contained 1–3 wt% of Al_2O_3. The BET specific surface area of the four milled and sieved waste glassy powders was between 0.37 m^2/g and 0.53 m^2/g.

The precursor, electric arc furnace slag (EAFS), used for alkali activation contains different amounts of SiO_2 and Al_2O_3 (16.8 wt % of SiO_2 and 8.1 wt% of Al_2O_3). Slag has a higher content of CaO (21.4 wt%) and MgO (16.8 wt%) than precursor used for Si and Al dissolution. The specific surface area of EAFS was 6.44 m^2/g. Based on one of our previous studies it is known that the mass percentage of amorphous phase in the slag is 63.2% (Češnovar et al., 2019).

Preparation and Characterisation of the Alternative Alkali Activators

Either 5 g or 20 g of the glassy waste powders were added to 200 ml of 10 M KOH solution, resulting in powder mass to 10 M KOH volume (m_{powder}/V_{KOH}) ratios of 0.025 g/ml and 0.1 g/ml, respectively. The 10 M KOH solution was prepared in the laboratory from distilled water and KOH flakes (Donau Chemie AG, Austria). The suspensions were left to boil at 120°C for either 4 h or 24 h, with constant mixing via a magnetic stirrer at 400 rpm. The suspensions were then cooled and filtered through a cellulose filter with a retention capacity of 4–12 μm (MN 640 m, (Macherey-Nagel GmbH & Co. KG, Germany). The filtrates obtained were later used as AAA solutions and analysed with regard to their Si and Al content via inductively coupled plasma-optical emission spectrometry (ICP-OES) (Varian, Model 715-ES).

For nuclear magnetic resonance (NMR) measurements, approximately 450 μl of each sample was transferred into 5 mm NMR tubes. Spectra were recorded on pure samples, using a coaxial insert with DMSO-d6 for the lock. The spectra were recorded on a Bruker Avance Neo 400 MHz NMR spectrometer (^{29}Si frequency 79.49 MHz) with a BBO Iprobe at 25°C. Spectra were recorded using a 30° pulse, 2s relaxation

TABLE 1 | The paste formulations, presented in terms of the mass percentages of the precursor and activator (wt%), and the nominal Si/Al and K/Al molar ratios.

	Precursor (wt%)	Activator (wt%)	Si/Al	K/Al
SW-KOH-4h-SLAG	67.0	33.0	1.6/1	2.3/1
SW-KOH-24h-SLAG	67.0	33.0	1.6/1	2.3/1
GW-KOH-4h-SLAG	67.0	33.0	1.6/1	2.3/1
GW-KOH-24h-SLAG	67.0	33.0	1.7/1	2.3/1
BG-KOH-4h-SLAG	67.0	33.0	1.6/1	2.3/1
BG-KOH-24h-SLAG	67.0	33.0	1.8/1	2.3/1
CRTG-KOH-4h-SLAG	67.0	33.0	1.6/1	2.3/1
CRTG-KOH-24 h-SLAG	67.0	33.0	1.7/1	2.3/1
Ref-10 M KOH-SLAG	67.0	33.0	1.5/1	2.3/1
Ref-K-Water glass-SLAG	68.8	31.2	3.0/1	1.2/1

delay and inverse gated decoupling. 4,000–10,000 scans were acquired per spectrum to obtain sufficient signal to noise. The spectra are referenced to the lock frequency and reported relative to TMS (δ_{Si} 0 ppm).

Preparation and Characterisation of the AAMs

The prepared AAAs were used in the alkali activation of the slag precursor in order to evaluate their effectiveness. The pastes were prepared using a constant AAA to precursor mass ratio. The paste formulations, presented in terms of the mass percentages of the precursor and activator (wt%), and the nominal Si/Al and K/Al molar ratios, are reported in **Table 1**. 150 g of slag was mixed with 74 g of AAA, giving a mass ratio m(AAA)/m(slag) of 0.49. Two reference slag specimens were prepared: a) 150.0 g of slag mixed with 74.0 g of 10 M KOH (m(KOH)/m(slag) = 0.49) and b) 150.0 g of slag mixed with 68.1 g of water glass (m(K-silicate)/m(slag) = 0.45). A commercially available K-silicate solution (K_2O; 15.4%, SiO_2; 30.4%, H_2O; 54.2%) was used as a reference alkali activator (potassium silicate Betol K 5020 T; Woellner Austria GmbH). The pastes were manually mixed for 2 min and then cast into silicon rubber moulds with dimensions of 20 × 20 × 80 mm^3. Pastes in the unsealed moulds were then put into a heating chamber, without controlling the relative humidity, for 72 h at temperature of 70°C in order to accelerate the alkali-activation process and thus harden the structure. The hardened binders were then demoulded, and the mechanical strength was measured. Mechanical strength (compressive and bending strength) was determined using a compressive and bending strength testing machine (ToniTechnik ToniNORM, Berlin, Germany, force application rate 0.05 kN/s). The bending strength of the various AAMs was assessed under three-point bending loading, while the compressive strength was assessed under compression loading using the two broken pieces from the bending test. The bending strength values reported represent the average results obtained from 3 test specimens of dimensions (20 × 20 × 80) mm^3. The compressive strength values reported represent the average results obtained from 5 test specimens.

The porosity of the hardened binders was analysed using a mercury-intrusion porosimeter (MIP; AutoPore IV 9500, Micromeritics, Norcross, USA) in the pressure range of 0.004–414 MPa. Before measurement, representative fragments of the AAMs with a volume of approximately 1 cm^3 were dried at 70°C in a heat chamber for 24 h.

Infrared spectra of the raw precursors and hardened binders were recorded using a Fourier transform infrared (FTIR) spectrometer (Spectrum Two, Perkin Elmer, USA), equipped with an attenuated total reflection accessory (Universal ATR) with a diamond/ZnSe crystal as a solid sample support, in the range from 400 cm^{-1}–4,000 cm^{-1} at a resolution of 4 cm^{-1}. The precursors were analysed as they were prepared for the alkali-activation process, whereas the hardened binders were ground before analysis.

Leaching tests were performed on the AAMs according to the European standard EN 12457-2 (2002). Depending on the moisture content of the sample, approximately 90 g of AAM, with a particle size of less than 4 mm, was added to deionized water in a glass bottle at a solid/liquid ratio of 1:10. The mixture was mixed on a tumbler at 10 rpm for 24 h at room temperature. It was then filtered to separate the solid fraction from the liquid fraction. The liquid fraction (leachate) was acidified with nitric acid to a pH of <2 in order to determine the amount of metals released via inductively coupled plasma mass spectrometry (ICP-MS, Agilent 7900). Following the leaching test, the pH (Mettler Toledo FiveEasy™ ph meter) and ionic conductivity (YOKOGAWA Model SC82) of the slag leachate and AAMs were measured. The concentration measured was comparable with Slovenia's national Decree on waste landfill based on the European Directive (Official Gazette of Republic Slovenia, 2014; Official Gazette of EU, 2018).

RESULTS AND DISCUSSION

Alternative Activators: The Solubility of Si and Al in 10 M KOH

The concentrations of dissolved silicon (Si), aluminium (Al) and calcium (Ca) ions for the four types of waste at different KOH concentrations, alongside the boiling time, are shown in **Table 3**. In general, the solubility of Si increases in line with an increasing solid content and boiling time. The solubility of Si was highest in the BG activator, i.e., 33.1 g/L after 24 h of boiling in KOH (solid content in a 0.1 g/ml suspension). Under the same conditions, the Si concentrations were 25 g/L and 17.9 g/L in the GW and CRTG

TABLE 2 | Analysis of the raw materials with respect to their chemical composition, presented as mass percentages in oxide form (wt%, XRF), specific surface area, and loss on ignition (LOI).

Oxide [wt%]	Waste glassy materials for the preparation of alternative activator solutions				Solid precursor
	SW	GW[a]	BG	CRTG	EAFS
Na_2O	3.85	15.31	13.47	7.61	0.13
MgO	11.70	4.10	1.68	0.46	14.87
Al_2O_3	16.09	3.11	0.91	2.07	8.54
SiO_2	43.60	65.44	72.37	58.49	21.05
K_2O	0.57	0.85	0.73	7.35	0.17
CaO	16.77	8.99	10.07	1.15	20.87
Fe_2O_3	5.34	0.73	0.21	0.16	11.37
BaO	—	0.05	0.07	7.72	0.017
SrO	—	—	1.02	7.34	0.03
PbO	—	—	0.06	3.92	0.017
LOI (550°C)	4.62	5.80	—	—	14.31
BET surface area [m^2/g]	0.37	0.44	0.45	0.53	6.44

[a]*Glass wool also contains B_2O_3, which cannot be determined by XRF. B_2O_3 content in glass wool is typically 3-9 wt% (Richet, 2021).*

activators, respectively. The highest concentration of dissolved Si in the BG activator is consistent with the highest amount of SiO_2 in the BG precursor. At a solid content of 0.025 g/L, the highest dissolved Si concentration (11.7 g/L) was observed in the GW activator after 24 h of thermal treatment. Similarly, after a short period of boiling (4 h), the highest dissolved Si concentration, 13.7 g/L, was obtained for GW dissolved in KOH, which was a little higher than the concentrations in the BG and CRTG activators, i.e., 10.9 g/L and 12.5 g/L, respectively. The concentration of Si in the SW activator was lower than in the other activators (4.3–6.1 g/L), which is related to the lower SiO_2 content and relatively high CaO and MgO content in the SW (XRF data in **Table 2**). As with the Si solubility, the Al solubility increases with an increasing solid content and boiling time, except in the case of SW. SW contains a far higher amount of Al than the other precursors used in this study (**Table 2**). The decrease in the amount of Al dissolved after 24 h of thermal treatment could be related to the precipitation of less soluble aluminosilicates in the KOH solutions, which is more obvious when the solid mass/volume ratio of the KOH activator is higher. With the exception of the CRTG samples, no Ca was measured at $m_{precursor}/m_{KOH}$ = 0.025 (the concentration was below the detection limit), and a lower concentration of Ca was measured in the SW, GW and BG AAAs at $m_{precursor}/m_{KOH}$ = 0.1 compared to the CRTG activator.

The comparison of these data shows that the dissolution of Si follows different kinetics in KOH than in NaOH. The data for dissolution in KOH and NaOH (König et al., 2020) are reported in **Table 3**. The dissolution behaviour of glass in alkali media is complex and related to multiple competing processes, e.g., network dissolution (hydrolysis), precipitation, and passivation (Maraghechi et al., 2016). In most cases, the content of dissolved Si is higher in KOH, with the difference being the highest in GW, BG and CRTG at longer dissolution times (24 h). A higher Si concentration in NaOH is, however, observed in GW at short dissolution times. According to the literature, the dissolution of aluminosilicate precursors is faster with KOH than with NaOH (Poulesquen et al., 2011). This could be explained by the fact that the K^+ ion is larger than Na^+, resulting in a more basic solution with a higher degree of solubilisation and polycondensation (Phair and Van Deventer, 2002). The higher pH of the solution leads to a higher concentration of monomers, due to the higher solubility of monomers in KOH (Khale and Chaudhary, 2007). The higher alkalinity increases the dissolution of Si, meaning the porous structure of the glass is exposed to a new surface and dissolution progresses (Newlands et al., 2017). Si-O-Si linkages are stronger than Si-O-Al and Al-O-Al bonds (de Jong and Brown, 1980; Xiao and Lasaga, 1994). Theoretical calculations show that the average bond length of Si-O bonds within Al-O-Si linkages increases when the Al/Si ratio is increased in the cluster, suggesting that hydrolysis of the Al-O-Si bonds becomes easier. This partially explains the higher dissolution at an increased Al/Si ratio, and preferential leaching of Al occurs more readily at a high Al/Si ratio (Hamilton et al., 2001). An increased Al content in the precursor will therefore lead to an increased rate of dissolution of the aluminosilicate material (Walkley et al., 2016). The alkali dissolution/precipitation reaction is controlled by the Si-rich Al-deficient surface precursor species at the mineral surface. Al preferentially dissolves from aluminosilicate glasses, any Si previously bound to Al is exposed, and the liberated Si dissolves (Oelkers and Gislason, 2001). XRF data shows that GW, CRTG and BG waste contain a similar amount of Si, with the highest amount found in the BG waste, whereas the highest amount of Al occurs in the SW. However, the solubility of Si in SW was not the highest considering the explanation above, where higher Al/Si ratio accelerates the solubility of Si. Moreover, regardless of the solid mass/KOH volume ratios, at a longer boiling time decreasing concentrations of Si and Al were observed in the SW activators but not in the other activators. This could be explained by the formation of various solid species (precipitation of a disordered phase could be present at a relatively high supersaturation (Gartner and Macphee, 2011)) that may precipitate at different equilibrium Al/Si ratios (Gasteiger et al., 1992). A decreasing Al and/or Si concentration may also be related to the accumulation of ions on the surface that disable or slow down the dissolution process. The ionized silanol group Si-O- on the surface attracts cations due to the re-absorption and

TABLE 3 | The concentrations of Si [g/L], Al [mg/L] and Ca [mg/L] in the alternative activators (AAAs) under different dissolution conditions. The numbers in brackets refer to dissolution in 10 M NaOH (König et al., 2020).

Dissolution conditions		SW-KOH activator			GW-KOH activator			BG-KOH activator			CRTG-KOH activator		
Boiling time [h]	m_{powder}/V_{NaOH} [g/ml]	c(Si) [g/L]	c(Al) [mg/L]	c(Ca) [mg/L]	c(Si) [g/L]	c(Al) [mg/L]	c(Ca) [mg/L]	c(Si) [g/L]	c(Al) [mg/L]	c(Ca) [mg/L]	c(Si) [g/L]	c(Al) [mg/L]	c(Ca) [mg/L]
4	**0.025**	4.3 (4)	1,472 (1,334)	<LOD	3.2 (6)	291 (310)	<LOD	3.1 (/)	56 (/)	<LOD	3.7 (/)	140 (/)	132
	0.1	5.9 (5)	1,566 (730)	14	13.7 (18)	579 (547)	24	10.9 (11)	172 (213)	19	12.5 (5)	407 (214)	118
24	**0.025**	6.1 (5)	762 (701)	<LOD	11.7 (6)	543 (326)	<LOD	7.6 (/)	126 (/)	<LOD	6.7 (/)	248 (/)	57
	0.1	4.3 (7)	308 (362)	10	25.6 (11)	831 (232)	31	33.1 (21)	528 (418)	54	17.9 (11)	534 (433)	76

formation of different unstable complexes (condensation process) that provide a barrier for further dissolution (Newlands et al., 2017) Al shows an inhibiting effect on dissolution by forming surface complexes (Chou and Wollast, 1985). The inhibitory effect of aqueous Al on dissolution could increase with increasing temperatures, due to the enhanced adsorption of cations onto surfaces with an increasing temperature (Chen and Brantley, 1997). KOH tends to leach out more calcium and magnesium than NaOH, although the solubility of Ca decreases at a higher pH. In a mixture of KOH/K-silicate, amorphous calcium silicate precipitates may form instead of alumina-silicate precipitates, and an increase in pH increases the concentrations of Ca, Al and Mg, but not that of Si. (Phair and Van Deventer, 2001). Other precursors used for the preparation of AAAs contain a far lower amount of Al and the gradual dissolution of Al cannot hinder the dissolution of Si through the formation of precipitates/surface complexes.

For further experiments, only samples with the ratio $m_{precursor}/V_{KOH}$ = 0.1 g/ml were selected (samples with a higher concentration of dissolved Si, with the exception of the SW).

Infrared Spectroscopy of the Alternative Activators

All FTIR spectra of the AAAs (**Figure 1**) show an absorption band in the region of 3,750–2,750 cm^{-1}, related to hydrogen-bonded OH groups, and a shoulder around 3,500 cm^{-1}, related to symmetric (ν_1) and asymmetric (ν_3) stretching vibrations of OH. Around 1,600 cm^{-1}, the bending band (ν_2) of H_2O can be seen. At about 800–1,000 cm^{-1}, in the silicate fingerprint region, there are visible peaks in the spectra of the samples with the concentration of dissolved Si ions above 10 g/L (peaks for the SW activator are not seen). Silicate solutions with a higher Si/M ratio (M = K, Na) or dilution level contain more polymerized species, observed as an increase in the wavenumber (Vidal et al., 2016). Between pH values of 11 and 14 the concentration of clusters (Q^3 and Q^4) in the solution decrease rapidly with an increasing pH, whereas the concentration of the Q^2 shifts progressively towards lower wavenumber values (Kamseu et al., 2017). Q^3 and Q^4 are present only in the K-silicate activator, and not in the AAAs prepared, as seen in **Figure 1**. Considering the data in **Table 3**, which shows the Si/K ratio in the slag-activator pastes prepared, it can be seen that the slag paste with the activator produced by thermally treating the BG in KOH for 24 h (BG_24h) has the highest Si/K ratio. It would therefore be expected that the position of that band was located at a higher wavenumber than the bands ascribed to the other AAAs. As seen in **Figure 1**, however, this is not the case, since the bands for the SW_4h and SW_24h activators, which have the lowest concentration of Si dissolved in KOH, are located at wavenumbers (984 cm^{-1}) higher than the other samples. The spectra of the other AAAs, prepared from BG, CRTG and SW, show bands in the range of 973–980 cm^{-1}. By increasing the pH, and thus decreasing the Si/M ratio, the Si-O-Si band displaces to a lower wavenumber, due to the appearance of SiO^- as a depolymerisation phenomenon (Vidal et al., 2016). The formation of various species with Si and Al may, however, have an important impact on the position of the bands in the infrared spectrum. Additional bands were observed in the spectra of all samples at about 930 cm^{-1}; the bands in the spectra of the SW activators are, however, barely visible. Those bands are assigned to the stretching of Si-O-Si bonds due to a depolymerisation phenomenon (Vidal et al., 2016). According to the literature, the most intensive peak of the Si-O-Si band in the K-silicate spectrum represents the Q^2 species (Kamseu et al., 2017), as presented in **Figure 1**. The peak intensity in the spectra of all AAAs is, however, much smaller, due to the lower amount of Si available in these samples compared to that in the commercially available alkali activator. Due to the low concentration of dissolved Si, and thus the low Si/K ratio, it is suggested that monomeric and dimeric silica species prevail in the AAAs prepared.

NMR Analysis of Alternative Activator Solutions

Figure 2 represents NMR spectra of the AAAs prepared in this study. N (0-4) in Q^n represents the number of bridging oxygens surrounding the Si atom, where Q^0 and Q^1 represent monomeric and dimeric silica (Vidal et al., 2016). ^{29}Si solution NMR spectra reveal that the silicate is mostly in low molecular weight forms in AAAs based on waste materials, with the monomeric (Q^0) species dominant in all of the samples (δ_{Si} -72 ppm). Two additional signals were observed in the spectra of most of the samples, corresponding to dimeric (Q^1, δ_{Si} -79 ppm) and cyclic trimeric (Q^2, δ_{Si} -82 ppm) species (Knight et al., 2007). These signals were not observed in the dissolved SW samples, due to the lower overall intensity of the peaks in the spectra of these samples

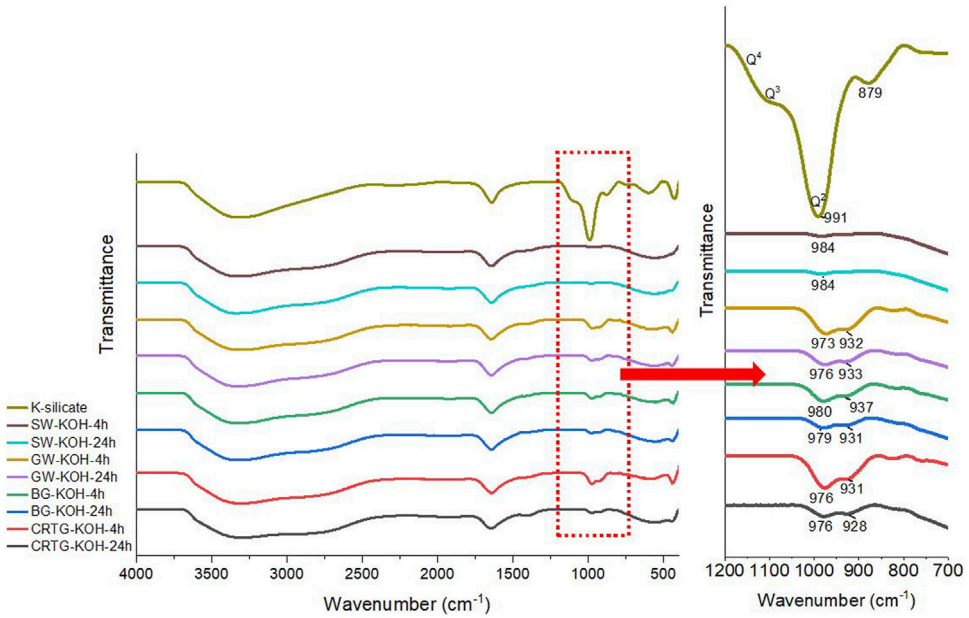

FIGURE 1 | FTIR spectra of the alternative activators based on 10 M KOH.

resulting from the lower concentrations of dissolved ions. Longer dissolution times increased the overall concentration of Si and the proportion of dimeric and trimeric species in CRTG and BG; (from approximately 20% of Si atoms in dimeric and trimeric form at 4 h to 30% at 24 h). For the SW and GW samples, longer dissolution times also increased the Si concentration, as shown by the integrals of signals in the respective NMR spectra, but proportion of species detected remained the same. In contrast, the ^{29}Si NMR spectrum of a commercial sample of K-silicate reveals a complex mixture of silicate species. Peaks corresponding to Q^0 (δ_{Si} −73 ppm), Q^1 (δ_{Si} -81 ppm), Q^2 (δ_{Si} −82 to −92 ppm), Q^3 (δ_{Si} −94 to −100 ppm) and Q^4 (δ_{Si} −102 to −109 ppm) tetrahedral sites were present, and the monomeric species represent only a minor fraction of silicon in the sample. Q^2 and Q^3 sites account for most of the silica species (39 and 43%, respectively). Q^2 and Q^3 are the principal species in solutions where the Si/M molar ratio >1 (Vidal et al., 2016). The precursor used for preparation of the AAAs and the silicates available in the solution are important factors affecting the alkali activation process and hardened performance (Alnahhal et al., 2021). The amount of dissolved Si, however, depends on the amorphous SiO_2 content in the precursor (Mejía et al., 2014; Tong et al., 2018). The optimum Si/M (M = Na, K) modulus could be in the range 1–2 indicating the Q^1 and Q^2 silica form (Luukkonen et al., 2018). The Q^n species depends on the amount of M_2O, whereby the Q^4 and Q^3 species decrease and Q^1 and Q^2 increase with an increasing content of M_2O (Malfait, 2009). When the Si/M molar ratio is above 1, the solutions mostly contain Q_2, Q_3 and Q_4 polymerized species, whereas when the ratio is below 1 the major species are Q_0 and Q_1 (Vidal et al., 2016). Parameters such as the SiO_2/M_2O molar ratio, the dilution level and the alkaline cation may, however, affect the presence of various silicate species. Specifically, an increase in the Si/M ratio and the dilution level of the silicate solution lead to a higher content of polymerized species, an influence that is more significant in the presence of KOH (Steins, 2014).

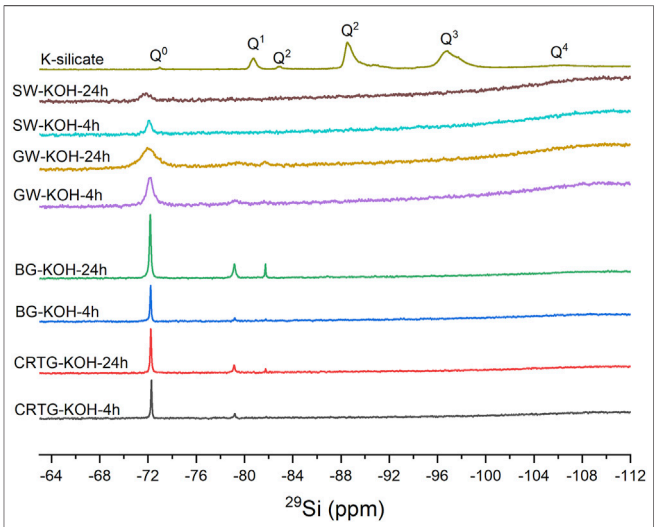

FIGURE 2 | ^{29}Si NMR spectra of the alternative activator samples.

Mechanical Properties of the Alkali-Activated Slag

The mechanical properties of the AAMs prepared based on KOH activators are shown in **Table 4**. The mechanical strengths of the AAMs vary, with compressive strength ranging from 3.09–9.47 MPa

TABLE 4 | Concentrations of dissolved Si and Al in the AAAs, the molar ratio of K/Al/Si in the prepared pastes, and the density, porosity and mechanical strength of the hardened slag (EAFS) binders. The K/Al/Si molar ratio in the prepared mixtures is calculated from the chemical composition obtained by XRF and XRD of the EAFS. The numbers in brackets refer to dissolution in NaOH (König et al., 2020).

Specimen name	Si concentration in the alternative activator [g/L]	Al concentration [g/L]	K/Al/Si molar ratio	Density [g/cm^3]	Open porosity [%] KOH (NaOH)	Total pore area [m^2/g]	Compressive strength [MPa]	Bending strength [MPa]
BG-KOH-4h-SLAG	10.9	0.17	2.3/1/1.6	1.77 ± 0.03	32.3 (40.5)	4.511	7.80 ± 0.60	3.35 ± 1.08
BG-KOH-24h-SLAG	33.1	0.53	2.3/1/1.8	2.00 ± 0.01	24.1 (39.7)	3.908	9.28 ± 1.04	2.79 ± 0.23
CRTG-KOH-4h-SLAG	12.5	0.41	2.3/1/1.6	1.84 ± 0.01	29.7 (43.5)	4.379	8.32 ± 0.61	3.89 ± 0.26
CRTG-KOH-24h-SLAG	17.9	0.53	2.3/1/1.7	1.92 ± 0.04	32.6 (42.3)	2.780	9.47 ± 1.34	2.59 ± 0.99
SW-KOH-4h-SLAG	5.9	1.57	2.3/1/1.6	1.77 ± 0.01	33.2 (42.2)	5.071	4.91 ± 0.43	2.91 ± 0.15
SW-KOH-24h-SLAG	4.3	1.47	2.3/1/1.6	1.68 ± 0.06	36.3 (41.1)	2.656	3.09 ± 2.79	1.92 ± 0.06
GW-KOH-4h-SLAG	13.7	0.58	2.3/1/1.6	1.89 ± 0.01	29.4 (40.6)	4.654	6.29 ± 0.81	3.20 ± 0.83
GW-KOH-24h-SLAG	25.6	0.83	2.3/1/1.7	1.97 ± 0.03	27.5 (40.6)	4.036	8.61 ± 0.78	3.36 ± 1.26
Ref_10 M KOH-SLAG	0	0	2.3/1/1.5	1.57 ± 0.03	40.9 (41.4)	3.223	1.97 ± 0.24	0.65 ± 0.53
Ref_K-silicate-SLAG	~200	0	1.2/1/3.0	1.89 ± 0.03	24.3 (24.8)	0.455	27.74 ± 5.88	10.77 ± 0.81

and bending strength between 1.92 and 3.89 MPa. The K-silicate-activated slag showed the highest compressive and bending strength (27.4 and 10.7 MPa, respectively), while the AAM prepared with 10 M KOH showed the lowest (1.97 and 0.65 MPa). The highest compressive strength (9.47 MPa) was measured in the sample produced from the CRTG activator obtained after 24 h of thermal treatment, resulting in a Si content of 17.9 g/L.

In the samples produced with AAAs, a trend of increasing compressive strength (denoted by circles) with an increasing concentration of dissolved Si in the AAAs occurs up to 17.9 g/L, as seen in **Figure 3**, while the values then saturate when the content of dissolved Si is higher (25.6 g/L and 33.1 g/L). A similar phenomenon with respect to the Si saturation—albeit in NaOH—was observed in the study by Bouchikhi et al. In their study, however, this phenomenon occurred at a higher precursor mass/NaOH solution volume ratio (30g/100 ml) (Bouchikhi et al., 2021). The increasing trend with the increasing concentration of dissolved Si in the AAAs is also observed in the bending strength of AAMs (denoted with circles) up to 12.5 g/L, as shown in **Figure 4**, reaching a maximum value of 3.9 MPa. Then, when the AAAs have higher Si concentrations, the values of bending strength range between 2.6 and 3.4 MPa. Since the slag contains a limited amount of amorphous phase, the amount of Si in the AAAs used for alkali activation of the slag is critically important to increase the mechanical strength of the hardened slag specimens (**Figures 3**, **4**). It is also shown in **Figure 4** that the density (denoted by triangles) of the hardened samples increases as the Si concentration increases. The increased density, i.e., a lower porosity in the samples, also contributes to better mechanical performance.

Comparison of KOH vs. NaOH

The samples prepared with KOH- and NaOH-based activators were prepared with waste glass and slag from the same batches. The mixture formulations were also the same. The influence of KOH or NaOH and their corresponding AAAs on the properties of the hardened samples can therefore be directly compared. Across all the AAA-mixtures, the compressive and bending strength of the hardened samples based on KOH are far higher than those based on NaOH, with the values being roughly 1–3-times higher (**Figure 5**). At the same time, the samples produced directly with 10 M KOH or 10 M NaOH have comparable mechanical properties, while the difference between the mechanical properties of the reference samples with silicate activators is of the order of 20%. Such a difference can be partly related to the higher density of the samples processed with KOH-based activators (**Figure 6**). We detected that these samples exhibited higher shrinkage after the hardening step.

The pH of the initial mixture of the alkali metal silicate and the precursor is the most important factor observed to control the compressive strength of the hardened matrix. With an increasing pH, there are more smaller chain oligomers and monomeric silicates which are more available to react with aluminium and calcium to form alkali-activated binding phase (Phair and Van Deventer, 2002). The compressive strength was greater in the K-Silicate/KOH activated matrices than in the Na-Silicate/NaOH activated matrices (Phair and Van Deventer, 2001). K^+ ion is more basic than Na^+ and allows higher rates of solubilized polymeric silicate ionization and dissolution. K^+ has a smaller hydration sphere than Na^+, which allows for more dense

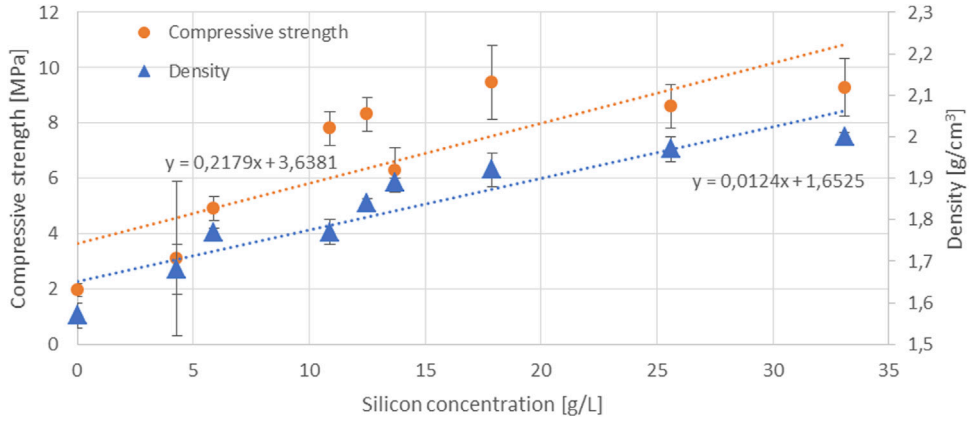

FIGURE 3 | Compressive strength and density of the hardened samples as a function of the Si concentration in the AAAs (circles denote compressive strength and triangles denote density).

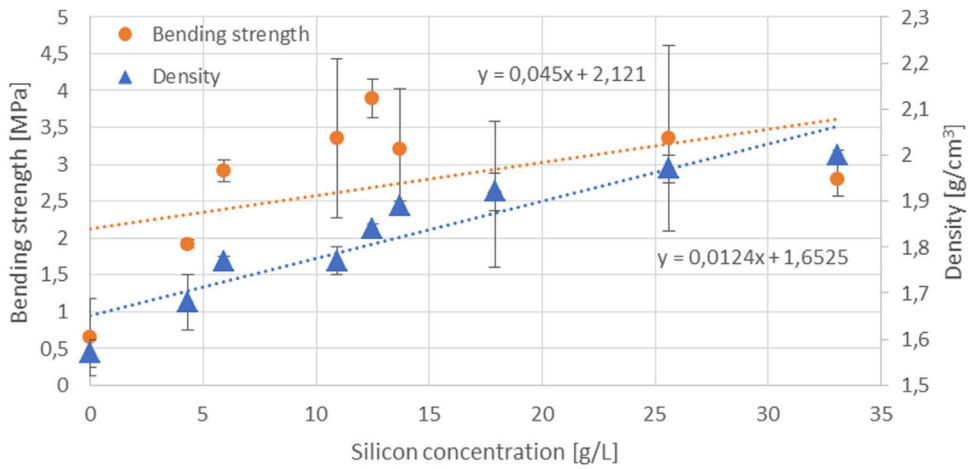

FIGURE 4 | Bending strength and density of the hardened samples as a function of the Si concentration in the AAAs (circles denote bending strength and triangles denote density).

polycondensation reactions, providing a greater overall network formation and an increase in the overall strength of the matrix (Phair et al., 2000). Alkali-activation using KOH is, however, slower than with NaOH, because K-alkali-activated gel is more disordered than Na-alkali-activated gel. K^+ ions have a greater tendency to interact with negatively charged [TO_4, T = Si, Al] units, thus limiting the condensation reaction. If NaOH is used as an activator, the alkali activation kinetics are faster, but the interactions between constituents are weaker and/or the formation of oligomers is more limited. If KOH is used as the activator, the reaction is slower, with far stronger interactions between constituents, resulting in better mechanical properties and a lower porosity (Phair and Van Deventer, 2001). KOH favours the formation of a three-dimensional structure, probably due to the greater connectivity between oligomers. However, this type of AAM is, therefore, more rigid (Poulesquen et al., 2011). Comparison with the reference sample prepared with K-silicate shows that the addition of K-silicate, which contains approximately 6–18 times more dissolved silica, results in a compressive strength 2.9–4.4-times higher than the AAMs prepared with SW-, GW-, BG- and CRTG-based AAAs. A similar relationship is found for the bending strength. The K-silicate reference has a molar ratio of Si/K > 1, and the increase in the Si/M ratio suggested the presence of more polymerized species in the solutions (Svensson et al., 1986), as observed by FTIR and NMR analysis (**Figures 1**, **2**). A higher Si/M ratio with more soluble silicate can accelerate the polycondensation reaction and thus result in the formation of more gel in the AAMs (Tchakouté et al., 2016b). The mechanical strength of the AAM with K-silicate is therefore the highest. The dissolved Si in the AAA influences the porosity, the formation of the gel, and the mechanical properties of the AAM, whereby the fast reaction of NaOH as an AAA may result in the formation of a more porous structure and thus a lower compressive strength,

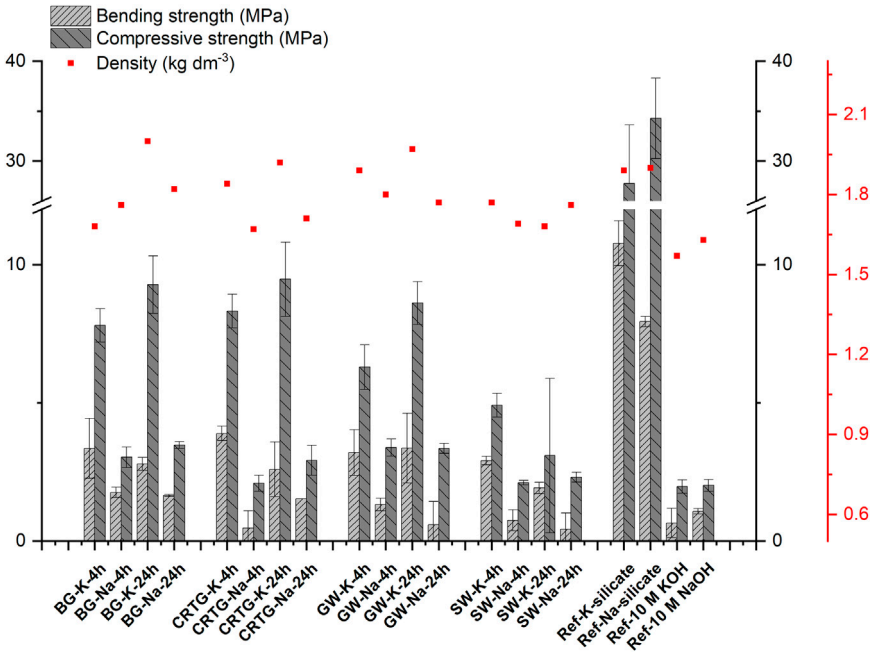

FIGURE 5 | Comparison of the a) compressive and b) bending strength of the hardened samples prepared by KOH- and NaOH-based AAAs.

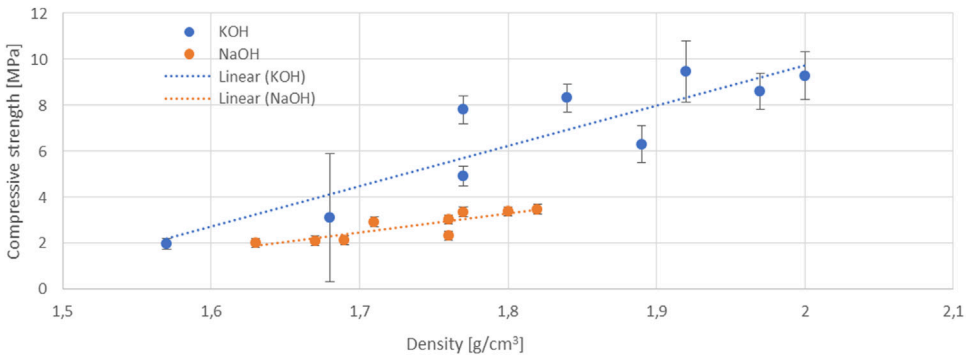

FIGURE 6 | Compressive strength of the hardened samples (from KOH- and NaOH-based AAAs) as a function of their density.

although the degree of reaction of the slag was comparable for the NaOH and Na-silicate (Haha et al., 2011). A lower Si/M (M = K, Na) ratio resulted in the formation of more pores in the structure (Tchakouté et al., 2016b). The kinetics of hydration significantly influences the porosity and compressive strength of the AAMs. AAMs prepared with NaOH had a higher porosity, due to the faster reaction and precipitation of products around the precursors at an early age (Ben Haha et al., 2011). The more porous structure of AAMs using NaOH-based activators was proven in one of our previous studies (König et al., 2020), and results showing the higher porosity in comparison to AAMs using KOH-based activators are shown in **Table 4**. There are no significant differences in the porosities of the samples activated with NaOH-based AAAs. The porosity of the AAMs activated with NaOH-based AAAs ranged between 39.7% and 43.5%, suggesting that, due to the faster reaction with NaOH, the amount of dissolved Si has a minor influence on the porosity and mechanical properties. Nevertheless, AAMs were observed to have a higher density, with more Si dissolved in the NaOH-based AAAs. In the KOH-based samples, a greater variation was observed between the porosities of the alkali-activated EAFS (24.1%–36.3%). This indicates that the dissolved Si has a greater influence on the porosity, density and mechanical properties. The CRTG_KOH_24h-SLAG sample shows the best mechanical properties, however, although the porosity is 32.6%, which is far higher than the BG_KOH_24h-SLAG sample that contains the highest amount of dissolved Si and a lower compressive strength. The contribution of Al to the development

of the gel structure in the early stages of the reaction plays an important role in the initial strength development of AAMs, due to the gel cross-linking and generating mechanical integrity, but the contribution of Si in the later stages of gel growth is known to be critical to strength development (Oelkers et al., 1994). The mechanical properties of the AAMs prepared in this study were therefore better when the amount of Si dissolved in the AAAs was higher. Consequently, the AAM sample prepared with 10 M KOH, without any dissolved Si, has the worst mechanical properties (**Table 4**).

FTIR Analyses of the Alkali-Activated Slag Samples

Figure 7 shows the FTIR spectra of the raw slag (EAFS) and the hardened alkali-activated binders. **Supplementary Table S2** shows the ratio of Si/Al in the prepared AAAs, Si/Al in the AAMs using AAAs, ratio of Ca/Si in the AAMs and the position of the Si-O-T asymmetric stretching bands. The raw slag spectrum has a broad band at 982 cm^{-1}, which corresponds to the asymmetric stretching vibrational mode of the TO_4 (T = Si, Al) tetrahedron (Yu et al., 1999). A major band is also observed at 1,417 cm^{-1}, corresponding to the vibrating modes of CO_3^{2-}, while a sharp peak at 875 cm^{-1} and barely visible peak at 713 cm^{-1} indicate the existence of a calcite phase. Following alkali activation, the asymmetric stretching vibration of Si–O-T (T = Si, Al) shifted from 982 cm^{-1} to 940–980 cm^{-1}, depending on the AAA used. In the K-silicate AAM (Ref_K-silicate), the band is positioned at 980 cm^{-1}, but this (Si–O-T band) shifts to lower values in the other samples, ranging between 940 $cm^{-1}$and 965 cm^{-1}. The position and intensity of the Si–O-T band indicate the degree of alkali activation (Chindaprasirt et al., 2009; Bernal et al., 2011). Broader peaks of all the spectra refer to a higher degree of heterogeneity in the sample and thus the existence of a broader range of different structural features. The shift to lower wavenumbers indicates a higher Al content in the AAM gel (i.e., a lower Si/Al ratio). The Si/Al ratios of the AAAs used in the alkali activation of EAFS are shown in **Supplementary Table S2**. More Al participates in the AAM gel structure when a higher amount of Si is available in the mix. A higher contribution of Si to AAM gels would, however, be expected when a higher amount of soluble Si was available in the early stages of the reaction (Hajimohammadi et al., 2011). In the present study, the highest amount of Al is present in the SW samples, which have the lowest concentration of Si. It follows that the Si/Al ratio was higher, more Al was available in the early stages of reaction, and the initially-formed AAM gel contained a high level of Al, resulting in the main band shifting to lower wavenumbers. When enough silica was released from the solid precursors used, and Si was incorporated into the gel structure, the main band shifted back to higher wavenumbers (Hajimohammadi et al., 2010). We did not, however, perform time-dependent sample measurements to prove this, but due to curing the samples for 3 days at 70°C, the position of the bands is final and no additional shift is expected. In the SW samples the bands are positioned at 951 cm^{-1} (4 h of thermal treatment, 5.9 g/L Si) and 940 cm^{-1} (24 h of treatment, 4.3 g/L Si), consistent with the lower Si/Al ratio of the AAAs. Bands are also observed at 940 cm^{-1} in CRTG after 24 h of treatment and GW after 4 h of thermal treatment, however, although the Si/Al ratios in these samples are significantly higher than that of the SW sample with 24 h of treatment. The shifts to lower wavenumbers observed could be due to the less polymerized AAM matrix in these samples, since there is no correlation with the Si/Al ratios. This is in contrast to the highest compressive strength of the CRTG-slag after 24 h of thermal treatment. A more homogenous AAM gel is observed as the availability of Si increases (Hajimohammadi et al., 2011). In the K-silicate AAM the Si-O-T band is positioned at 982 cm^{-1}, whereas in BG, which has the highest amount of dissolved Si, it is located at 965 cm^{-1}. In KOH-activated slag the band occurs at 962 cm^{-1}. This sample has the lowest mechanical properties and the highest porosity, suggesting a highly depolymerised matrix. Since the mechanical properties increase with a higher amount of Si, polymerization should improve in all the samples prepared from AAAs. There should be other mechanisms for formation of the matrix, due to variation in the position of the bands. A band (shoulder) at around 1,050 cm^{-1} is related to unreacted EAFS particles in the mixture. This band is not observed in samples 1_BG-KOH-4h-SLAG and 2_BG-KOH-24h-SLAG, which have the highest amount of dissolved Si. Bands in the range 1,423–1,435 cm^{-1} represent stretching vibration of the O-C-O bond (CO_3^{2-}). In all samples except the K-silicate and BG AAMs, an additional shoulder observed at around 1,370 cm^{-1} representing the high level of carbonation process due to the non-uniform nature of their microstructure (Yusuf et al., 2014). In a previous study

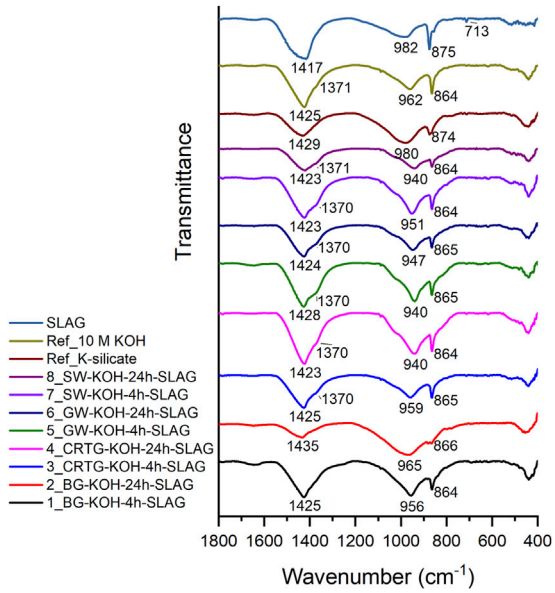

FIGURE 7 | FTIR spectra of the hardened binders composed of alkali-activated slag after curing for 72 h at 70°C.

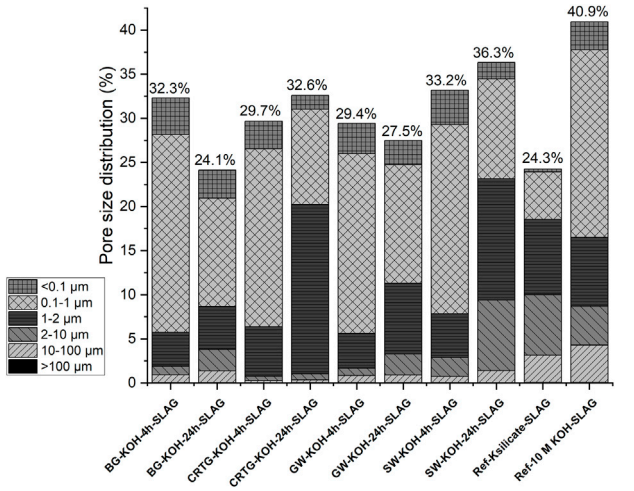

FIGURE 8 | Stacked graph showing the pore size distribution of hardened alkali-activated slag samples after curing for 72 h at 70°C.

Lancellotti et al. (2021) proposed that C-S-H is formed in alkali-activated EAFS slag. The degree of polymerization depends on the Ca/Si ratio, with higher polymerization occurring when Ca/Si<1.25 (Macphee et al., 1988). With high alkalinity, the carbonation of gel favours silicate polymerization (Black et al., 2007; Garbev et al., 2007) modification of gel, and a redistribution of Ca to surface sites (García Lodeiro et al., 2009). Since C–S–H gel reacts with atmospheric CO_2, a high degree of carbonation is present in the samples, as is observed from the intensive bands occurring at around 1,400 cm^{-1} and 865 cm^{-1}.

Hg Porosity Analyses of the Alkali-Activated Slag Samples

The pore dimensions of the alkali-activated slags, measured by MIP, are shown in **Figure 8** and **Supplementary Figure S2**, with the raw data provided in **Table 4**. The pore sizes of the AAM samples prepared with AAAs are similar to those prepared with 10 M KOH. The reference sample prepared using K-silicate has noticeably larger pores, but the total open porosity is lower (24%). The open porosity of the samples ranges between 24% and 41%. The lowest open porosities were shown in the slag specimen activated by K-silicate and the BG-KOH-24h-SLAG sample, which has the highest content of dissolved Si, whereas the highest open porosity was measured in the sample alkali-activated by 10 M KOH. The higher porosity of the KOH-activated samples is due to a faster initial reaction between the activator and the slag, leading to a coarser microstructure and poorly distributed hydration product (dense C-S-H gel). In the silicate activator, the hydration of slag is slower, and the hydration product is distributed uniformly, resulting in a more homogenous microstructure and consequently a lower porosity and higher compressive strength (Ben Haha et al., 2011). The mechanical properties of AAMs were therefore highest in the case of pure K-silicate, with a higher Si/K ratio and more polymerized species, as also confirmed by the shift of Si-O-T (T = Si, Al) at 982 cm^{-1} in the alkali-activated EAFS (**Figure 7**). At 24%, however, the porosity was similar to that of the BG-KOH-24h-SLAG sample, which had the lowest porosity; the position of the band located at 965 cm^{-1} indicates a less polymerized aluminosilicate matrix, although it is still more than all of the other alkali-activated samples. The formation of different hydration products at the same porosity influences the strength of various materials (Jin et al., 2021). Interestingly, the CRTG-KOH-24h-SLAG sample, which had the highest compressive strength, did not have the lowest porosity. Compared to the other samples in **Figure 8**, this sample has a far higher proportion of pores between 1 and 2 µm, which might have an influence to the mechanical properties.

Leaching Test Results

Leaching tests were performed on the AAMs to assess the newly-proposed AAA solutions from an environmental point of view. **Table 5** shows the concentrations of toxic trace and minor elements in AAAs prepared with a $m_{precursor}/m_{KOH}$ ratio of 0.1 g/ml. The concentrations of elements in the AAAs analysed were mostly below the upper limits for non-toxic materials, with the exception of Ba, Pb, Sb and Zn. This was, however, not the case in all AAAs, and was most evident in the AAAs prepared from CRTG. Pb and Ba are present in the original waste material in amounts of 7.7 wt% and 3.9 wt%, respectively, Zn represents 0.5 wt%, while Sb was not identified by XRF due to the lower concentration. Other AAAs did not show elevated concentrations of these elements. The BG and GW activators, however, show elevated concentrations of As.

Furthermore, leaching tests were performed on samples activated with AAAs and EAFS in order to determine the leaching/immobilisation potential of elements, especially of those present in higher concentrations in the alkali activated CRTG waste (Ba, Pb, Sb and Zn). **Table 6** shows the concentrations of toxic elements present in the leachates of the AAMs prepared. Leaching tests were performed on AAMs prepared using eight different AAAs ($m_{precursorr}/m_{KOH}$ ratio of 0.1 g/ml) and EAFS. Slag activated with 10 M KOH and K-silicate served as references. Slag was additionally evaluated for leaching prior to alkali activation to assess the results obtained. The last two rows of the table show the limits according to legislation for inert and non-hazardous waste. The leachate concentrations of the elements of environmental concern (As, Ba, Cd, Cr, Cu, Hg, Mo, Ni, Pb, Sb, Se, and Zn) presented in **Tables 5**, **6** were evaluated with respect to the Decree on the Landfilling of Wastes, which outlines criteria for waste of a specific type (inert, non-hazardous, and hazardous) intended for landfill (Decree on waste landfill (Official Gazette of Republic Slovenia, 2014; Official Gazette of EU, 2018).

TABLE 5 | Concentrations of toxic trace and minor elements in AAAs prepared AAAs with a $m_{precursor}/m_{KOH}$ ratio of 0.1 g/ml.

Sample	As (mg/L)	Ba (mg/L)	Cd (mg/L)	Cr (mg/L)	Cu (mg/L)	Hg (mg/L)	Mo (mg/L)	Ni (mg/L)	Pb (mg/L)	Sb (mg/L)	Se (mg/L)	Zn (mg/L)
1_BG-KOH-4h	0.61	2.02	0.002	0.20	0.06	0.001	0.17	0.02	2.00	0.14	0.04	2.00
2_BG-KOH-24h	1.40	13.0	0.01	0.26	0.04	0.001	0.25	0.01	18.1	0.78	0.13	3.83
3_CRTG-KOH-4h	0.14	170	0.01	<LOD	0.06	<LOD	0.09	0.09	1,130	142	0.03	70.8
4_CRTG-KOH-24h	0.19	145	0.01	0.001	0.06	<LOD	0.09	0.05	1,580	179	0.04	88.2
5_GW-KOH-4h	0.58	2.90	0.001	0.01	0.10	0.001	0.48	0.19	1.78	0.19	<LOD	3.71
6_GW-KOH-24h	0.85	1.43	0.01	0.02	0.03	0.001	0.73	0.12	0.41	0.32	<LOD	4.09
7_SW-KOH-4h	0.07	3.04	<LOD	0.01	0.13	<LOD	0.08	0.10	0.74	0.04	<LOD	2.82
8_SW-KOH-24h	0.14	2.05	0.001	0.02	0.02	<LOD	0.16	0.07	0.53	0.07	<LOD	2.74
Inert material[a]	0.05	2	0.004	0.05	0.2	0.001	0.05	0.04	0.05	0.006	0.01	0.4
Non-hazardous material[a]	0.2	10	0.3	1	5	0.02	1	1	10	0.07	0.05	5

[a]*Decree on waste landfill.*

TABLE 6 | The concentrations of 12 elements measured in leachates in leaching experiments performed following the SIST EN:12457-2 standard protocol.

	As (mg/kg)	Ba (mg/kg)	Cd (mg/kg)	Cr (mg/kg)	Cu (mg/kg)	Hg (mg/kg)	Mo (mg/kg)	Ni (mg/kg)	Pb (mg/kg)	Sb (mg/kg)	Se (mg/kg)	Zn (mg/kg)
BG-KOH-4h-SLAG	2.28	0.01	0.05	116	0.25	0.013	45.8	0.02	0.08	0.22	0.50	0.03
BG-KOH-24h-SLAG	0.60	0.02	0.01	20.4	0.47	0.007	11.5	0.08	0.04	0.12	0.16	0.02
CRTG-KOH-4h-SLAG	1.81	0.02	0.04	113	0.04	0.007	45.5	0.01	0.18	5.37	0.43	< LOD
CRTG-KOH-24h-SLAG	2.60	0.03	0.05	157	0.03	0.010	54.8	0.01	1.58	5.71	0.53	0.08
GW-KOH-4h-SLAG	2.66	0.01	0.05	97.5	0.05	0.013	51.3	0.02	0.11	0.48	0.40	0.04
GW-KOH-24h-SLAG	2.96	0.01	0.05	80.2	0.07	0.016	53.4	0.02	0.10	0.29	0.39	0.05
SW-KOH-4h-SLAG	2.57	0.01	0.05	143	0.03	0.010	51.7	0.01	0.12	0.22	0.48	0.05
SW-KOH-24h-SLAG	2.78	0.01	0.05	172	0.02	0.010	55.3	0.01	0.22	0.18	0.50	0.07
K-silicate-KOH-SLAG	0.27	0.02	0.01	16.1	0.03	0.006	6.43	0.01	0.01	0.06	0.09	0.03
10 M KOH-SLAG	1.64	0.01	0.04	120	0.02	0.011	39.2	0.01	0.02	0.28	0.27	0.02
EAFS (slag)	0.003	0.35	0.004	7.5	0.01	0.005	3.27	0.001	0.004	0.02	< LOD	0.01
Inert material[a]	0.5	20	0.04	0.5	2	0.01	0.5	0.4	0.5	0.06	0.1	4
Non-hazardous material[a]	2	100	3	10	50	0.2	10	10	10	0.7	0.5	50

[a]*Decree on waste landfill.*

Pb, Sb, Ba and Zn occur at elevated concentrations in the CRTG AAAs (**Table 5**), but a significant decrease in the concentration of all four elements could be seen in the leachates of AAMs. Based on the concentrations of the AAM leachates (**Table 6**) compared to those in the AAAs, it can be seen that Sb was highly immobilized by the alkali activation process. Of all the elements with elevated concentrations in the CRTG-based AAAs it was, however, the only element where the concentration still exceeded the allowable values for non-hazardous waste. On the other hand, three other critical elements (As, Cr and Mo) exceeded the permitted values for non-hazardous material following alkali activation with EAFS, with the values of Cr and Mo being especially high. Looking at the concentrations of elements in the slag leachates (**Table 6**), it can be seen that all concentrations are below the permitted values for non-toxic material. Although the pH value of the solution was slightly above 11, it is evident that the slag itself did not contribute to the elevated concentrations of As, Cr and Mo at that pH value. Leachates of solutions other than slag have a pH of above 13.3 in all AAMs, however, since all the AAAs prepared have a pH of over 14 (due to the use of 10 M KOH for their preparation). It is seen in **Table 6** that not all AAM samples show the same trend with respect to the leaching of As, Cr, Mo and Sb. Ref-K-silicate, for example shows significantly lower concentrations of these elements, which could be related to the lower pH of the

TABLE 7 | The pH and ionic conductivity values of the AAM samples prepared and the slag before alkali activation.

	pH	Conductivity (mS cm^{-1})
BG-4h-SLAG	13.54	25.1
BG-24h-SLAG	13.36	15.3
CRTG-4h-SLAG	13.42	24.1
CRTG-24h-SLAG	13.68	31.6
GW-4h-SLAG	13.66	27.8
GW-24h-SLAG	13.67	28.5
SW-4h-SLAG	13.72	29.5
SW-24h-SLAG	13.82	33.5
Ref-K-silicate-SLAG	13.14	9.10
Ref 10 M KOH-SLAG	13.50	23.8
EAFS	11.17	0.59

activator and the more polymerized matrix of the alkali-activated EAFS. The concentration of elements measured in the BG-24h-KOH-SLAG sample was also similar. The Si content, however, is 6-times lower than that of the K-silicate, and it is expected that less matrix is formed in the BG-KOH-24h-SLAG sample. Since the porosity of both samples is the same, better immobilisation occurs in the K-silicate AAM, as shown by the lower concentrations of elements seen in **Table 6**. The better immobilisation of elements in the BG-KOH-24h-SLAG compared to the alkali-activated samples could be due to the greater amount of matrix formed in the AAM and the slightly lower pH compared to the other samples, as observed in **Table 7**. Microstructural damage may also affect the leaching of toxic elements.

The leaching characteristics of metals from slag are strongly related to the structure and chemical composition of the slag. Due to the reduction condition during smelting, the elements are zerovalent or occur in more reduced valence states, mainly incorporated in the spinel structure (oxides of the form (M^{2+}) $(Fe^{3+})_2O_4$ where M^{2+} and Fe^{3+} are the divalent and trivalent cations occupying tetrahedral and octahedral interstitial positions in the lattice formed by O^{2-}), and the elements are leached as more reduced species (Cornelis et al., 2008). Concentrations of some toxic elements exceeding legislative limits in the leachates of alkali-activated EAFS (where Na-silicate was used for alkali activation) were found in the study by Lancellotti et al. (2021). The concentrations of Sb and As released from the AAMs remained below regulation limits, while an increasing amount of Mo was leached, presenting values which slightly exceed the limit for non-hazardous landfill waste (Lancellotti et al., 2021). During alkali activation, however, the pH significantly increases and may affect the leaching potential of some elements (when activated with a silicate activator rather than hydroxide the pH is lower). AAMs are able to effectively decrease the mobility of cationic species, whereas transition metals, which form oxyanionic species, remain less effectively stabilized (Bernal et al., 2014a; Bernal et al., 2014b). Physical encapsulation, e.g., the zeolite-type cage structures, can trap hazardous components if their size is suitable. Other types of physical encapsulation can take place when a physical barrier prevents the leaching medium (water) from contacting the hazardous components, thus preventing leaching (Luukkonen et al., 2019). Metal(loid)s can react with other reactive compounds in the mixture and become part of the aluminosilicate structure, for example by replacing silicon atoms (Schoenung, 2008). The immobilization of metals does not occur with ion exchange but rather through isomorphous substitution (Zheng et al., 2016). At a very high pH, however, the speciation of transition metal oxides will favour the formation of far more soluble oxide or hydroxide compounds [38].

Considering the study by Loncnar et al., where a pH-dependent model was adjusted to different ladle slag samples, a higher leaching potential was observed for Cr and Mo at pH > 12, while the leaching of Ba reduced (Loncnar et al., 2016). The elements As, Cr, Mo, Sb and Se can form oxyanions in solution, forming a range of different species depending on both pH and redox potential, and, due to their high solubility, could be found in relatively high concentrations in leachates compared to the cationic species (Cornelis et al., 2008). Elements present in their elemental state, hydroxides, and oxides formed by reduced species at a high pH are only slightly soluble (Cr(III), Sb(III) (Beverskog and Puigdomenech, 1997; Séby et al., 2001; Filella and May, 2003). Although Cr(III) is present in steel slag, soluble Cr is mostly in the hexavalent form (Chaurand et al., 2006), which is the form predominantly found in leachates (Kersten et al., 1997). Similarly, it was shown in the study by Shen et al. (2004) that almost all of the total Cr in the leachate was present in the form of Cr(VI), since equilibrium with insoluble Ca–Cr(III) minerals cause the $Cr(OH)_4^-$ concentration to be very low, meaning that soluble Cr is almost always hexavalent. Cr is mainly present in the form of oxides, while Ni and Mo are in the form of metal (Shen et al., 2004). The reduction of Cr(VI) into **c**ationic Cr(III) with Fe(II) or S^{2-} balances the negatively charged Al tetrahedra in the AAMs (Sun et al., 2014; Chen et al., 2017). The high Si/Al molar ratio was found to reduce leaching of Cr and Cu as the higher strength of Si-O-Si over the Si-O-Al bond decreases depolymerization during leaching (Zheng et al., 2010). The leaching behaviour of As, Cr, Se and Sb is highly dependent on the redox state at which they occur in the solid, whereas Mo is insensitive to this. In addition to leachability, with minerals containing Ca there could also be surface adsorption and solid solution formation, which would reduce the leaching (Cornelis et al., 2008). The concentration of Se in the sample leachates of the CRTG-24h-SLAG exceeded the upper limit for non-hazardous waste, whereas a high amount of Sb is immobilized following alkali activation, and, in the present work, Sb(III) is the expected form of Sb in the AAMs. However, Sb still exceeded the limit for non-hazardous waste in both CRTG samples. When using very reactive precursors with a high amount of amorphous aluminosilicates and/or Ca (e.g., GGBFS, metakaolin, fly ash), immobilization may improve due to the formation of more matrices. This was confirmed in our previous study, where high mechanical strengths were obtained in alkali activated fly ash (using AAAs prepared in NaOH solution), even when the amounts of dissolved Si and Al were low (König et al., 2020).

In highly alkaline solutions, Pb is capable of combining with either a negatively charged hydroxide or silicate species (Phair and Van Deventer, 2001). The cation is likely to combine with hydroxide, which is more labile and easily reacts with it (Phair and Van Deventer, 2001). More silicate species are available at a

pH of 12 and cations are more likely to react with them (polysilicate anions), whereas more hydroxide ions exist at a pH of 14 which preferably react with them (e.g., as $Pb(OH)_2$ or $Pb(OH)^-$ (Huang et al., 1987)). Because they exist as anions, however, they are unable to bind with polysilicate or any polysialate framework, and those cations that bound with silicate at a high pH will most likely be in monomeric silicate form (Phair and Van Deventer, 2001). In the study by Palacios and Palomo, Pb was found in the Pb_3SiO_5 phase (Palacios and Palomo, 2004). The leachability of Cu(II) and Pb(II) from the alkali-activated matrix decreased as the pH of the activating solution increased (Phair et al., 2004). AAMs could therefore immobilise and stabilise high proportions of Pb, as could be seen in the present study, especially in the case of the CRTG activator (**Tables 5**, **6**). Cu is not a problematic element in the present study, and according to the literature it is more or less distributed throughout the aluminosilicate gel binder phase (Van Jaarsveld et al., 1999). The leaching kinetics of the immobilised Pb were in accordance with a diffusion mechanism. Since we were not able to confirm the presence of Pb_3SiO_5 in the CRTG-activated samples through XRD analysis (the results are not shown in the present work), it is suggested that the immobilisation of Pb in our system is a combination of physical encapsulation and chemical bonding, in which adsorption also plays an important role (Van Jaarsveld et al., 1998). Pb is immobilised (stabilised) in AAM through the formation of a network-forming element replacing Si; Pb(II) ions balance the negatively charged Al tetrahedra (physical immobilization), and insoluble $Pb(OH)_2$ can be encapsulated into the alkali activated structure (Ogundiran et al., 2013) by bonding to the silicate chain through oxide and/or hydroxide links (Van Jaarsveld and van Deventer, 1999). Since the CRTG-KOH-24h-SLAG has the highest mechanical properties, a moderate porosity, unclear FTIR spectra, and not the highest amount of Si dissolved in the AAAs, Pb could have an important but unknown role in the matrix. The concentration of As exceeded legislative limits in all of the AAM leachates with the exception of the BG-KOH-24h, ref-K-silicate and ref-KOH samples. In the AAAs higher concentrations were measured in the BG and GW activators (**Table 5**), whereas in the CRTG and SW samples elevated concentrations of As in the leachates come from EAFS following the alkali activation process. In BG and GW, however, the concentrations of As reduce below the upper limit for non-hazardous material in the BG-KOH-24h sample. Zn, which was found in elevated concentrations in the CRTG AAAs, is effectively immobilised in the highly alkaline AAM matrix. Zinc can form covalent Zn-O-Si bonds, and so will eventually become substituted into the silicate chains of a calcium silicate hydrate once the system reaches the point of setting (Anseau et al., 2005). Low calcium AAMs can, however, be a good matrix for the immobilization of this metal. EAFS contains less than 20 wt% Ca and does not belong to the low-Ca binders, but due to the very low concentrations of Zn found in the leachates of all the samples prepared, it seems that immobilisation is possible even when higher amounts of Ca are present. Some studies suggest that compressive strength decreases when Zn is introduced to AAMs. In OPC, for example, Ca–Zn interactions lead to the precipitation of calcium zincate on the surface (Pereira et al., 2009). It is known that impurities (elements) from Si-rich wastes affect the compressive strength through the presence of side reactions during alkali activation (He et al., 2013). Additional studies are, however, needed to investigate the influence of Zn (and other toxic elements) on the mechanical properties, as well as the immobilisation mechanism in EAFS activated systems.

CONCLUSION

AAAs were prepared from SW, GW, BG, and CRTG, through dissolution in a 10 M KOH solution, as a potential substitute for commercial alkali silicates. The amounts of Si and Al ions dissolved in the filtrates, as determined by ICP-OES, depended on the time of thermal treatment, and ranged from 4.3–33.1 g/L and 0.06–1.57 g/L, respectively. The highest concentration of dissolved Si was almost 50% higher than the highest value observed when a 10 M NaOH solution was used in one of our previous studies. The NMR spectra of the AAAs indicate the presence of Q^0, Q^1, and Q^2 species, except in the case of the SW activators, where Q^2 could not be identified due to the low concentration of Si dissolved in the KOH solution. However, the FTIR spectra of the AAAs show two bands, at 973–984 cm^{-1} and around 930 cm^{-1}, while K-silicate shows the band at 991 cm^{-1}. The solutions prepared were then used to prepare alkali-activated samples using EAFS as the precursor material. Properties of the cured samples were compared with those of two reference samples, prepared using the slag and either 10 M KOH or commercial K-silicate solution. The compressive and bending strengths of the cured samples prepared with AAAs reached 9.5 and 3.9 MPa, respectively, which are 2–5 times higher than those of the sample prepared with 10 M KOH. Conversely, the strengths of the samples prepared with K-silicate were 2.5–3 times higher than those of the samples prepared with AAAs. The porosity of the AAMs prepared with KOH activators ranged from 24.1%–40.9%, with the lowest porosity measured in the BG-KOH-24h-SLAG sample (24.1%). The compressive strength values obtained for the samples prepared with KOH-based activators are far better (2–5 times higher) than the values obtained for samples prepared with NaOH-based activators. Part of this difference can be attributed to the higher density of the samples prepared with KOH, which is due to the slower reaction, better polymerization and consequently the formation of a larger matrix compared to NaOH. The results of the leaching tests show elevated concentrations of As, Cr and Mo in leachates of alkali-activated EAFS, considering the legislation data. Mix designs using AAAs and EAFS should be modified in the future to decrease the amount of toxic trace elements in leachates of AAMs. However, the AAMs prepared with EAFS and AAAs show good potential for the immobilisation Ba, Pb, Sb, and Zn. Further studies should be carried out to obtain more detailed information about the matrix and the Si/Al and Ca/Si ratios, as well as the distribution of toxic elements such as Pb using SEM-EDXS. In this way, we will obtain important information that will

help in interpreting the leaching/immobilisation of toxic elements from AAMs.

DATA AVAILABILITY STATEMENT

The original contributions presented in the study are included in the article/**Supplementary Material**, further inquiries can be directed to the corresponding author.

AUTHOR CONTRIBUTIONS

Conceptualization and methodology: MP, KK, and VD; Formal analysis and data curation: MP, KK, JK, and UJ; Writing—original draft preparation: KK, MP; Writing—review and editing: MP, KK, JK, UJ, and VD; Supervision: VD.

ACKNOWLEDGMENTS

We acknowledge financial support from the Slovenian Research Agency, Slovenia, through project No. Z2-3199 »The immobilisation and leaching of toxic trace elements in alkali-activated materials prepared from locally available waste and by-products«, and program P2-0273 »Building structures and materials«. JK also acknowledges the support from the Slovenian Research Agency (grant number L2-9221).

SUPPLEMENTARY MATERIAL

The Supplementary Material for this article can be found online at: https://www.frontiersin.org/articles/10.3389/fmats.2022.902139/full#supplementary-material

REFERENCES

Adesanya, E., Perumal, P., Luukkonen, T., Yliniemi, J., Ohenoja, K., Kinnunen, P., et al. (2021). Opportunities to Improve Sustainability of Alkali-Activated Materials: A Review of Side-Stream Based Activators. *J. Clean. Prod.* 286, 125558. doi:10.1016/j.jclepro.2020.125558

Alnahhal, M. F., Kim, T., and Hajimohammadi, A. (2021). Waste-derived Activators for Alkali-Activated Materials: A Review. *Cem. Concr. Compos.* 118, 103980. doi:10.1016/j.cemconcomp.2021.103980

Alonso, M. M., Gascó, C., Morales, M. M., Suárez-Navarro, J. A., Zamorano, M., and Puertas, F. (2019). Olive Biomass Ash as an Alternative Activator in Geopolymer Formation: A Study of Strength, Radiology and Leaching Behaviour. *Cem. Concr. Compos.* 104, 103384. doi:10.1016/j.cemconcomp.2019.103384

Anseau, M. R., Leung, J. P., Sahai, N., and Swaddle, T. W. (2005). Interactions of Silicate Ions with Zinc(II) and Aluminum(III) in Alkaline Aqueous Solution. *Inorg. Chem.* 44 (22), 8023–8032. doi:10.1021/ic050594c

Bagheri, A., and Moukannaa, S. (2021). A New Approach to the Reuse of Waste Glass in the Production of Alkali-Activated Materials. *Clean. Eng. Technol.* 4, 100212. doi:10.1016/j.clet.2021.100212

Ben Haha, M., Le Saout, G., Winnefeld, F., and Lothenbach, B. (2011). Influence of Activator Type on Hydration Kinetics, Hydrate Assemblage and Microstructural Development of Alkali Activated Blast-Furnace Slags. *Cem. Concr. Res.* 41 (3), 301–310. doi:10.1016/j.cemconres.2010.11.016

Bernal, S. A., Provis, J. L., Fernández-Jiménez, A., Krivenko, P. V., Kavalerova, E., Palacios, M., et al. (2014a). "Binder Chemistry - High-Calcium Alkali-Activated Materials," in *Alkali Activated Materials* (Dordrecht: Springer), 59–91. doi:10.1007/978-94-007-7672-2_3

Bernal, S. A., Provis, J. L., Rose, V., and Mejía de Gutierrez, R. (2011). Evolution of Binder Structure in Sodium Silicate-Activated Slag-Metakaolin Blends. *Cem. Concr. Compos.* 33 (1), 46–54. doi:10.1016/j.cemconcomp.2010.09.004

Bernal, S. A., San Nicolas, R., Myers, R. J., de Gutiérrez, M. R., Puertas, F., van Deventer, J. S. J., et al. (2014b). MgO Content of Slag Controls Phase Evolution and Structural Changes Induced by Accelerated Carbonation in Alkali-Activated Binders. *Cem. Concr. Res.* 57, 33–43. doi:10.1016/j.cemconres.2013.12.003

Beverskog, B., and Puigdomenech, I. (1997). Revised Pourbaix Diagrams for Chromium at 25-300 °C. *Corros. Sci.* 39 (1), 43–57. doi:10.1016/s0010-938x(97)89244-x

Black, L., Breen, C., Yarwood, J., Garbev, K., Stemmermann, P., and Gasharova, B. (2007). Structural Features of C–S–H(i) and its Carbonation in Air—A Raman Spectroscopic Study. Part II: Carbonated Phases. *J Am. Ceram. Soc.* 90 (3), 908–917. doi:10.1111/j.1551-2916.2006.01429.x

Boca Santa, R. A. A., Soares, C., and Riella, H. G. (2017). Geopolymers Obtained from Bottom Ash as Source of Aluminosilicate Cured at Room Temperature. *Constr. Build. Mater.* 157, 459–466. doi:10.1016/j.conbuildmat.2017.09.111

Bouchikhi, A., Mamindy-Pajany, Y., Maherzi, W., Albert-Mercier, C., El-Moueden, H., Benzerzour, M., et al. (2021). Use of Residual Waste Glass in an Alkali-Activated Binder - Structural Characterization, Environmental Leaching Behavior and Comparison of Reactivity. *J. Build. Eng.* 34, 101903. doi:10.1016/j.jobe.2020.101903

Bouzón, N., Payá, J., Borrachero, M. V., Soriano, L., Tashima, M. M., and Monzó, J. (2014). Refluxed Rice Husk ash/NaOH Suspension for Preparing Alkali Activated Binders. *Mater. Lett.* 115, 72–74. doi:10.1016/j.matlet.2013.10.001

Češnovar, M., Traven, K., Horvat, B., and Ducman, V. (2019). The Potential of Ladle Slag and Electric Arc Furnace Slag Use in Synthesizing Alkali Activated Materials; the Influence of Curing on Mechanical Properties. *Mater. (Basel)* 12 (7), 1173. doi:10.3390/ma12071173

Chaurand, P., Rose, J., Domas, J., and Bottero, J-Y. (2006). Speciation of Cr and V within BOF Steel Slag Reused in Road Constructions. *J. Geochem. Explor* 88 (1–3), 10–14. doi:10.1016/j.gexplo.2005.08.006

Chen, J., Wang, Y., Zhou, S., and Lei, X. (2017). Reduction/immobilization Processes of Hexavalent Chromium Using Metakaolin-Based Geopolymer. *J. Environ. Chem. Eng.* 5 (1), 373–380. doi:10.1016/j.jece.2016.11.028

Chen, Y., and Brantley, S. L. (1997). Temperature- and pH-Dependence of Albite Dissolution Rate at Acid pH. *Chem. Geol.* 135 (3), 275–290. doi:10.1016/s0009-2541(96)00126-x

Chindaprasirt, P., Jaturapitakkul, C., Chalee, W., and Rattanasak, U. (2009). Comparative Study on the Characteristics of Fly Ash and Bottom Ash Geopolymers. *Waste Manag.* 29 (2), 539–543. doi:10.1016/j.wasman.2008.06.023

Chou, L., and Wollast, R. (1985). Steady-state Kinetics and Dissolution Mechanisms of Albite. *Am. J. Sci.* 285 (10), 963–993. doi:10.2475/ajs.285.10.963

Cornelis, G., Johnson, C. A., Van Gerven, T. V., and Vandecasteele, C. (2008). Leaching Mechanisms of Oxyanionic Metalloid and Metal Species in Alkaline Solid Wastes: A Review. *Appl. Geochem.* 23 (5), 955–976. doi:10.1016/j.apgeochem.2008.02.001

de Jong, B. H. W. S., and Brown, G. E. (1980). Polymerization of Silicate and Aluminate Tetrahedra in Glasses, Melts and Aqueous Solutions-II. The Network Modifying Effects of Mg^{2+} , K^+, Na^+, Li^+, H^+, OH^-, F^-, Cl^-, H_2O, CO_2 and H_3O^+ on Silicate Polymers. *Geochimica Cosmochimica Acta* 44 (11), 1627–1642. doi:10.1016/0016-7037(80)90216-1

de Moraes Pinheiro, S. M., Font, A., Soriano, L., Tashima, M. M., Monzó, J., Borrachero, M. V., et al. (2018). Olive-stone Biomass Ash (OBA): An Alternative Alkaline Source for the Blast Furnace Slag Activation. *Constr. Build. Mater.* 178, 327–338. doi:10.1016/j.conbuildmat.2018.05.157

Diedrich, T., Dybowska, A., Schott, J., Valsami-Jones, E., and Oelkers, E. H. (2012). The Dissolution Rates of SiO2 Nanoparticles as a Function of Particle Size. *Environ. Sci. Technol.* 46 (9), 4909–4915. doi:10.1021/es2045053

El-Naggar, M. R., and El-Dessouky, M. I. (2017). Re-use of Waste Glass in Improving Properties of Metakaolin-Based Geopolymers: Mechanical and

Microstructure Examinations. *Constr. Build. Mater.* 132, 543–555. doi:10.1016/j.conbuildmat.2016.12.023

Filella, M., and May, P. M. (2003). Computer Simulation of the Low-Molecular-Weight Inorganic Species Distribution of Antimony(III) and Antimony(V) in Natural Waters. *Geochimica Cosmochimica Acta* 67 (21), 4013–4031. doi:10.1016/s0016-7037(03)00095-4

Font, A., Soriano, L., Moraes, J. C. B., Tashima, M. M., Monzó, J., Borrachero, M. V., et al. (2017). A 100% Waste-Based Alkali-Activated Material by Using Olive-Stone Biomass Ash (OBA) and Blast Furnace Slag (BFS). *Mater Lett.* 203, 46–49. doi:10.1016/j.matlet.2017.05.129

Garbev, K., Stemmermann, P., Black, L., Breen, C., Yarwood, J., and Gasharova, B. (2007). Structural Features of C–S–H(i) and its Carbonation in Air—A Raman Spectroscopic Study. Part I: Fresh Phases. *J Am. Ceram. Soc.* 90 (3), 900–907. doi:10.1111/j.1551-2916.2006.01428.x

García Lodeiro, I., Macphee, D. E., Palomo, A., and Fernández-Jiménez, A. (2009). Effect of Alkalis on Fresh C-S-H Gels. FTIR Analysis. *Cem. Concr. Res.* 39 (3), 147–153. doi:10.1016/j.cemconres.2009.01.003

Gartner, E. M., and Macphee, D. E. (2011). A Physico-Chemical Basis for Novel Cementitious Binders. *Cem. Concr. Res.* 41 (7), 736–749. doi:10.1016/j.cemconres.2011.03.006

Gasteiger, H. A., Frederick, W. J., and Streisel, R. C. (1992). Solubility of Aluminosilicates in Alkaline Solutions and a Thermodynamic Equilibrium Model. *Ind. Eng. Chem. Res.* 31 (4), 1183–1190. doi:10.1021/ie00004a031

Geraldo, R. H., Fernandes, L. F. R., and Camarini, G. (2017). Water Treatment Sludge and Rice Husk Ash to Sustainable Geopolymer Production. *J. Clean. Prod.* 149, 146–155. doi:10.1016/j.jclepro.2017.02.076

Habert, G., d'Espinose de Lacaillerie, J. B., and Roussel, N. (2011). An Environmental Evaluation of Geopolymer Based Concrete Production: Reviewing Current Research Trends. *J. Clean. Prod.* 19 (11), 1229–1238. doi:10.1016/j.jclepro.2011.03.012

Haha, M. B., Lothenbach, B., Le Saout, G., and Winnefeld, F. (2011). Influence of Slag Chemistry on the Hydration of Alkali-Activated Blast-Furnace Slag - Part I: Effect of MgO. *Cem. Concr. Res.* 41 (9), 955–963. doi:10.1016/j.cemconres.2011.05.002

Hajimohammadi, A., Provis, J. L., and van Deventer, J. S. J. (2010). Effect of Alumina Release Rate on the Mechanism of Geopolymer Gel Formation. *Chem. Mat.* 22 (18), 5199–5208. doi:10.1021/cm101151n

Hajimohammadi, A., Provis, J. L., and van Deventer, J. S. J. (2011). The Effect of Silica Availability on the Mechanism of Geopolymerisation. *Cem. Concr. Res.* 41 (3), 210–216. doi:10.1016/j.cemconres.2011.02.001

Hamilton, J. P., Brantley, S. L., Pantano, C. G., Criscenti, L. J., and Kubicki, J. D. (2001). Dissolution of Nepheline, Jadeite and Albite Glasses: toward Better Models for Aluminosilicate Dissolution. *Geochimica Cosmochimica Acta* 65 (21), 3683–3702. doi:10.1016/s0016-7037(01)00724-4

He, J., Jie, Y., Zhang, J., Yu, Y., and Zhang, G. (2013). Synthesis and Characterization of Red Mud and Rice Husk Ash-Based Geopolymer Composites. *Cem. Concr. Compos.* 37, 108–118. doi:10.1016/j.cemconcomp.2012.11.010

Heath, A., Paine, K., and McManus, M. (2014). Minimising the Global Warming Potential of Clay Based Geopolymers. *J. Clean. Prod.* 78, 75–83. doi:10.1016/j.jclepro.2014.04.046

Huang, C. P., Hsieh, Y. S., Park, S. W., Ozden Corapcioglu, M., and Bowers, A. R. (1987). "Chemical Interactions between Heavy Metal Ions and Hydrous Solids," in *Metals speciation, separation and recovery*. Chelsea, MI: Lewis Pub Inc, 437–465.

Jiang, M., Chen, X., Rajabipour, F., and Hendrickson, C. T. (2014). Comparative Life Cycle Assessment of Conventional, Glass Powder, and Alkali-Activated Slag Concrete and Mortar. *J. Infrastruct. Syst.* 20 (4), 4014020. doi:10.1061/(asce)is.1943-555x.0000211

Jin, S., Zhou, J., Zhao, X., and Sun, L. (2021). Quantitative Relationship between Pore Size Distribution and Compressive Strength of Cementitious Materials. *Constr. Build. Mater.* 273, 121727. doi:10.1016/j.conbuildmat.2020.121727

Kamseu, E., Beleuk à Moungam, L. M., Cannio, M., Billong, N., Chaysuwan, D., Melo, U. C., et al. (2017). Substitution of Sodium Silicate with Rice Husk Ash-NaOH Solution in Metakaolin Based Geopolymer Cement Concerning Reduction in Global Warming. *J. Clean. Prod.* 142, 3050–3060. doi:10.1016/j.jclepro.2016.10.164

Kersten, M., Christoph Moor, H., and Johnson, C. A. (1997). Speciation of Trace Metals in Leachate from a MSWI Bottom Ash Landfill. *Appl. Geochem.* 12 (5), 675–683. doi:10.1016/s0883-2927(97)00022-x

Khale, D., and Chaudhary, R. (2007). Mechanism of Geopolymerization and Factors Influencing its Development: a Review. *J. Mater Sci.* 42 (3), 729–746. doi:10.1007/s10853-006-0401-4

Knight, C. T. G., Balec, R. J., and Kinrade, S. D. (2007). The Structure of Silicate Anions in Aqueous Alkaline Solutions. *Angew. Chem.* 119 (43), 8296–8300. doi:10.1002/ange.200702986

König, K., Traven, K., Pavlin, M., and Ducman, V. (2020). Evaluation of Locally Available Amorphous Waste Materials as a Source for Alternative Alkali Activators. *Ceram. Int.* 47, 4864–4873. doi:10.1016/j.ceramint.2020.10.059

Kvočka, D., Lešek, A., Knez, F., Ducman, V., Panizza, M., Tsoutis, C., et al. (2020). Life Cycle Assessment of Prefabricated Geopolymeric Façade Cladding Panels Made from Large Fractions of Recycled Construction and Demolition Waste. *Mater. (Basel)* 13 (18), 3931. doi:10.3390/ma13183931

Lancellotti, I., Piccolo, F., Traven, K., Češnovar, M., Ducman, V., and Leonelli, C. (2021). Alkali Activation of Metallurgical Slags: Reactivity, Chemical Behavior, and Environmental Assessment. *Materials* 14, 639. doi:10.3390/ma14030639

Leonelli, C., Turk, J., Poggetto, G. D., Catauro, M., Traven, K., Mauko Pranjić, A., et al. (2022). Environmental and Biological Impact of Fly Ash and Metakaolin-Based Alkali-Activated Foams Obtained at 70°C and Fired at 1,000°C. *Front. Chem.* 10, 845452. doi:10.3389/fchem.2022.845452

Loncnar, M., van der Sloot, H. A., Mladenovič, A., Zupančič, M., Kobal, L., and Bukovec, P. (2016). Study of the Leaching Behaviour of Ladle Slags by Means of Leaching Tests Combined with Geochemical Modelling and Mineralogical Investigations. *J. Hazard. Mater.* 317, 147–157. doi:10.1016/j.jhazmat.2016.05.046

Luukkonen, T., Abdollahnejad, Z., Yliniemi, J., Kinnunen, P., and Illikainen, M. (2018). One-part Alkali-Activated Materials: A Review. *Cem. Concr. Res.* 103, 21–34. doi:10.1016/j.cemconres.2017.10.001

Luukkonen, T., Heponiemi, A., Runtti, H., Pesonen, J., Yliniemi, J., and Lassi, U. (2019). Application of Alkali-Activated Materials for Water and Wastewater Treatment: a Review. *Rev. Environ. Sci. Biotechnol.* 18 (2), 271–297. doi:10.1007/s11157-019-09494-0

Macphee, D. E., Lachowski, E. E., and Glasser, F. P. (1988). Polymerization Effects in C-S-H: Implications for Portland Cement Hydration. *Adv. Cem. Res.* 1 (3), 131–137. doi:10.1680/1988.1.3.131

Malfait, W. J. (2009). Quantitative Raman Spectroscopy: Speciation of Cesium Silicate Glasses. *J. Raman Spectrosc.* 40 (12), 1895–1901. doi:10.1002/jrs.2338

Maraghechi, H., Rajabipour, F., Pantano, C. G., and Burgos, W. D. (2016). Effect of Calcium on Dissolution and Precipitation Reactions of Amorphous Silica at High Alkalinity. *Cem. Concr. Res.* 87, 1–13. doi:10.1016/j.cemconres.2016.05.004

McLellan, B. C., Williams, R. P., Lay, J., van Riessen, A., and Corder, G. D. (2011). Costs and Carbon Emissions for Geopolymer Pastes in Comparison to Ordinary Portland Cement. *J. Clean. Prod.* 19 (9), 1080–1090. doi:10.1016/j.jclepro.2011.02.010

Mejía, J. M., Mejía de Gutiérrez, R., and Puertas, F. (2014). Rice Husk Ash as a Source of Silica in Alkali-Activated Fly Ash and Granulated Blast Furnace Slag Systems. *Mater. De. Construcción* 63 (311), 361–375. doi:10.3989/mc.2013.04712

Mendes, B. C., Pedroti, L. G., Vieira, C. M. F., Marvila, M., Azevedo, A. R. G., Franco de Carvalho, J. M., et al. (2021). Application of Eco-Friendly Alternative Activators in Alkali-Activated Materials: A Review. *J. Build. Eng.* 35, 102010. doi:10.1016/j.jobe.2020.102010

Moraes, J. C. B., Tashima, M. M., Akasaki, J. L., Melges, J. L. P., Monzó, J., Borrachero, M. V., et al. (2016). Increasing the Sustainability of Alkali-Activated Binders: The Use of Sugar Cane Straw Ash (SCSA). *Constr. Build. Mater.* 124, 148–154. doi:10.1016/j.conbuildmat.2016.07.090

Newlands, K. C., Foss, M., Matchei, T., Skibsted, J., and Macphee, D. E. (2017). Early Stage Dissolution Characteristics of Aluminosilicate Glasses with Blast Furnace Slag- and Fly-ash-like Compositions. *J. Am. Ceram. Soc.* 100 (5), 1941–1955. doi:10.1111/jace.14716

Oelkers, E. H., and Gislason, S. R. (2001). The Mechanism, Rates and Consequences of Basaltic Glass Dissolution: I. An Experimental Study of the Dissolution Rates of Basaltic Glass as a Function of Aqueous Al, Si and Oxalic Acid Concentration at 25°C and pH = 3 and 11. *Geochimica Cosmochimica Acta* 65 (21), 3671–3681. doi:10.1016/s0016-7037(01)00664-0

Oelkers, E. H., Schott, J., and Devidal, J.-L. (1994). The Effect of Aluminum, pH, and Chemical Affinity on the Rates of Aluminosilicate Dissolution Reactions. *Geochimica Cosmochimica Acta* 58 (9), 2011–2024. doi:10.1016/0016-7037(94)90281-x

Official Gazette of Eu (2018). Directive (EU) 2018/851 of the European Parliament and of the Council of 30 May 2018 Amending Directive 2008/98/EC on Waste [Internet]. Available from: https://eur-lex.europa.eu/legal-content/EN/TXT/?uri=celex%3A32018L0851. (Accessed May 5, 2022).

Official Gazette of Republic Slovenia (2014). Decree on Waste Landfill, Nos. 2020, 10/14, 54/15, 36/16, 37/18 [Internet]. Available from: https://www.ecolex.org/details/legislation/decree-on-the-landfill-of-waste-lex-faoc130542/. (Accessed May 5, 2022).

Ogundiran, M. B., Nugteren, H. W., and Witkamp, G. J. (2013). Immobilisation of Lead Smelting Slag within Spent Aluminate-Fly Ash Based Geopolymers. *J. Hazard. Mater.* 248-249, 29–36. doi:10.1016/j.jhazmat.2012.12.040

Ouellet-Plamondon, C., and Habert, G. (2015). "Life Cycle Assessment (LCA) of Alkali-Activated Cements and Concretes," in *Chindaprasirt Mortars and Concretes PBT-H of A-AC*. Editors F. Pacheco-Torgal, J. A. Labrincha, C. Leonelli, and A. Palomo (Oxford: Woodhead Publishing), 663–686. doi:10.1533/9781782422884.5.663

Palacios, M., and Palomo, A. (2004). Alkali-activated Fly Ash Matrices for Lead Immobilisation: a Comparison of Different Leaching Tests. *Adv. Cem. Res.* 16 (4), 137–144. doi:10.1680/adcr.2004.16.4.137

Pavlin, M., Horvat, B., Frankovič, A., and Ducman, V. (2021). Mechanical, Microstructural and Mineralogical Evaluation of Alkali-Activated Waste Glass and Stone Wool. *Ceram. Int.* 47, 15102–15113. doi:10.1016/j.ceramint.2021.02.068

Pereira, C. F., Luna, Y., Querol, X., Antenucci, D., and Vale, J. (2009). Waste Stabilization/solidification of an Electric Arc Furnace Dust Using Fly Ash-Based Geopolymers. *Fuel* 88 (7), 1185–1193. doi:10.1016/j.fuel.2008.01.021

Phair, J. W., and Van Deventer, J. S. J. (2002). Effect of the Silicate Activator pH on the Microstructural Characteristics of Waste-Based Geopolymers. *Int. J. Min. Process* 66 (1), 121–143. doi:10.1016/s0301-7516(02)00013-3

Phair, J. W., and Van Deventer, J. S. J. (2001). Effect of Silicate Activator pH on the Leaching and Material Characteristics of Waste-Based Inorganic Polymers. *Miner. Eng.* 14 (3), 289–304. doi:10.1016/s0892-6875(01)00002-4

Phair, J. W., van Deventer, J. S. J., and Smith, J. D. (2004). Effect of Al Source and Alkali Activation on Pb and Cu Immobilisation in Fly-Ash Based "geopolymers". *Appl. Geochem.* 19 (3), 423–434. doi:10.1016/s0883-2927(03)00151-3

Phair, J. W., Van Deventer, J. S. J., and Smith, J. D. (2000). Mechanism of Polysialation in the Incorporation of Zirconia into Fly Ash-Based Geopolymers. *Ind. Eng. Chem. Res.* 39 (8), 2925–2934. doi:10.1021/ie990929w

Poulesquen, A., Frizon, F., and Lambertin, D. (2011). Rheological Behavior of Alkali-Activated Metakaolin during Geopolymerization. *J. Non-Crystalline Solids* 357 (21), 3565–3571. doi:10.1016/j.jnoncrysol.2011.07.013

Puertas, F., and Torres-Carrasco, M. (2014). Use of Glass Waste as an Activator in the Preparation of Alkali-Activated Slag. Mechanical Strength and Paste Characterisation. *Cem. Concr. Res.* 57, 95–104. doi:10.1016/j.cemconres.2013.12.005

Richet, P. (2021). (Editior). *Encyclopedia of Glass Science, Technology, History, and Culture*. Hoboken, NJ: John Wiley & Sons. doi:10.1002/9781118801017

Rodríguez, E. D., Bernal, S. A., Provis, J. L., Paya, J., Monzo, J. M., and Borrachero, M. V. (2013). Effect of Nanosilica-Based Activators on the Performance of an Alkali-Activated Fly Ash Binder. *Cem. Concr. Compos.* 35 (1), 1–11. doi:10.1016/j.cemconcomp.2012.08.025

Schoenung, J. M. (2008). "Lead Compounds," in *Ceramic and Glass Materials* (Boston, MA: Springer), 151–167. doi:10.1007/978-0-387-73362-3_9

Séby, F., Potin-Gautier, M., Giffaut, E., Borge, G., and Donard, O. F. X. (2001). A Critical Review of Thermodynamic Data for Selenium Species at 25 C. *Chem. Geol.* 171 (3–4), 173–194. doi:10.1016/s0009-2541(00)00246-1

Shen, H., Forssberg, E., and Nordström, U. (2004). Physicochemical and Mineralogical Properties of Stainless Steel Slags Oriented to Metal Recovery. *Resour. Conservation Recycl.* 40 (3), 245–271. doi:10.1016/s0921-3449(03)00072-7

Soriano, L., Font, A., Tashima, M. M., Monzó, J., Borrachero, M. V., and Payá, J. (2020). One-part Blast Furnace Slag Mortars Activated with Almond-Shell Biomass Ash: A New 100% Waste-Based Material. *Mater Lett.* 272, 127882. doi:10.1016/j.matlet.2020.127882

Steins, P. (2014). *Influence des paramètres de formulation sur la texturation et la structuration des géopolymères*. Français: Limoges.

Sun, T., Chen, J., Lei, X., and Zhou, C. (2014). Detoxification and Immobilization of Chromite Ore Processing Residue with Metakaolin-Based Geopolymer. *J. Environ. Chem. Eng.* 2 (1), 304–309. doi:10.1016/j.jece.2013.12.022

Svensson, I. L., Sjöberg, S., and Öhman, L.-O. (1986). Polysilicate Equilibria in Concentrated Sodium Silicate Solutions. *J. Chem. Soc. Faraday Trans. 1* 82 (12), 3635–3646. doi:10.1039/f19868203635

Tchakouté, H. K., Rüscher, C. H., Kong, S., Kamseu, E., and Leonelli, C. (2016a). Geopolymer Binders from Metakaolin Using Sodium Waterglass from Waste Glass and Rice Husk Ash as Alternative Activators: A Comparative Study. *Constr. Build. Mater.* 114, 276–289. doi:10.1016/j.conbuildmat.2016.03.184

Tchakouté, H. K., Rüscher, C. H., Kong, S., and Ranjbar, N. (2016b). Synthesis of Sodium Waterglass from White Rice Husk Ash as an Activator to Produce Metakaolin-Based Geopolymer Cements. *J. Build. Eng.* 6, 252–261. doi:10.1016/j.jobe.2016.04.007

Tong, K. T., Vinai, R., and Soutsos, M. N. (2018). Use of Vietnamese Rice Husk Ash for the Production of Sodium Silicate as the Activator for Alkali-Activated Binders. *J. Clean. Prod.* 201, 272–286. doi:10.1016/j.jclepro.2018.08.025

Torres-Carrasco, M., Palomo, J. G., and Puertas, F. (2014). Sodium Silicate Solutions from Dissolution of Glasswastes. Statistical Analysis. *Mater Construcción* 64 (314), e014. doi:10.3989/mc.2014.05213

Torres-Carrasco, M., and Puertas, F. (2015). Waste Glass in the Geopolymer Preparation. Mechanical and Microstructural Characterisation. *J. Clean. Prod.* 90, 397–408. doi:10.1016/j.jclepro.2014.11.074

Turner, L. K., and Collins, F. G. (2013). Carbon Dioxide Equivalent (CO2-e) Emissions: A Comparison between Geopolymer and OPC Cement Concrete. *Constr. Build. Mater.* 43, 125–130. doi:10.1016/j.conbuildmat.2013.01.023

Van Jaarsveld, J. G. S., Van Deventer, J. S. J., and Lorenzen, L. (1998). Factors Affecting the Immobilization of Metals in Geopolymerized Flyash. *Metall Materi Trans B* 29 (1), 283–291. doi:10.1007/s11663-998-0032-z

Van Jaarsveld, J. G. S., Van Deventer, J. S. J., and Schwartzman, A. (1999). The Potential Use of Geopolymeric Materials to Immobilise Toxic Metals: Part II. Material and Leaching Characteristics. *Miner. Eng.* 12 (1), 75–91. doi:10.1016/s0892-6875(98)00121-6

Van Jaarsveld, J. G. S., and van Deventer, J. S. J. (1999). The Effect of Metal Contaminants on the Formation and Properties of Waste-Based Geopolymers. *Cem. Concr. Res.* 29 (8), 1189–1200. doi:10.1016/s0008-8846(99)00032-0

Vidal, L., Joussein, E., Colas, M., Cornette, J., Sanz, J., Sobrados, I., et al. (2016). Controlling the Reactivity of Silicate Solutions: A FTIR, Raman and NMR Study. *Colloids Surfaces A Physicochem. Eng. Aspects* 503, 101–109. doi:10.1016/j.colsurfa.2016.05.039

Villaquirán-Caicedo, M. A. (2019). Studying Different Silica Sources for Preparation of Alternative Waterglass Used in Preparation of Binary Geopolymer Binders from Metakaolin/boiler Slag. *Constr. Build. Mater.* 227, 116621. doi:10.1016/j.conbuildmat.2019.08.002

Vinai, R., and Soutsos, M. (2019). Production of Sodium Silicate Powder from Waste Glass Cullet for Alkali Activation of Alternative Binders. *Cem. Concr. Res.* 116, 45–56. doi:10.1016/j.cemconres.2018.11.008

Walkley, B., San Nicolas, R., Sani, M.-A., Gehman, J. D., van Deventer, J. S. J., and Provis, J. L. (2016). Phase Evolution of Na2O-Al2O3-SiO2-H2o Gels in Synthetic Aluminosilicate Binders. *Dalton Trans.* 45 (13), 5521–5535. doi:10.1039/C5DT04878H

Xiao, Y., and Lasaga, A. C. (1994). Ab Initio quantum Mechanical Studies of the Kinetics and Mechanisms of Silicate Dissolution: H+(H3O+) Catalysis. *Geochimica Cosmochimica Acta* 58 (24), 5379–5400. doi:10.1016/0016-7037(94)90237-2

Yang, K.-H., Song, J.-K., and Song, K.-I. (2013). Assessment of CO2 Reduction of Alkali-Activated Concrete. *J. Clean. Prod.* 39, 265–272. doi:10.1016/j.jclepro.2012.08.001

Yu, P., Kirkpatrick, R. J., Poe, B., McMillan, P. F., and Cong, X. (1999). Structure of Calcium Silicate Hydrate (C-S-H): Near-, Mid-, and Far-Infrared Spectroscopy. *J. Am. Ceram. Soc.* 82 (3), 742–748. doi:10.1111/j.1151-2916.1999.tb01826.x

Yusuf, M. O., Johari, M. A. M., Ahmad, Z. A., and Maslehuddin, M. (2014). Performance of Different Grades of Palm Oil Fuel Ash with Ground Slag as Base Materials in the Synthesis of Alkaline Activated Mortar. *J. Adv. Concr. Technol.* 12 (10), 378–387. doi:10.3151/jact.12.378

Zheng, L., Wang, W., and Gao, X. (2016). Solidification and Immobilization of MSWI Fly Ash through Aluminate Geopolymerization: Based on Partial Charge Model Analysis. *Waste Manag.* 58, 270–279. doi:10.1016/j.wasman.2016.08.019

Zheng, L., Wang, W., and Shi, Y. (2010). The Effects of Alkaline Dosage and Si/Al Ratio on the Immobilization of Heavy Metals in Municipal Solid Waste Incineration Fly Ash-Based Geopolymer. *Chemosphere* 79 (6), 665–671. doi:10.1016/j.chemosphere.2010.02.018

Živica, V. (2006). Effectiveness of New Silica Fume Alkali Activator. *Cem. Concr. Compos* 28 (1), 21–25. doi:10.1016/j.cemconcomp.2005.07.004

Conflict of Interest: The authors declare that the research was conducted in the absence of any commercial or financial relationships that could be construed as a potential conflict of interest.

The handling editor declared a past co-authorship with one of the author VD.

Publisher's Note: All claims expressed in this article are solely those of the authors and do not necessarily represent those of their affiliated organizations, or those of the publisher, the editors and the reviewers. Any product that may be evaluated in this article, or claim that may be made by its manufacturer, is not guaranteed or endorsed by the publisher.

Copyright © 2022 Pavlin, König, König, Javornik and Ducman. This is an open-access article distributed under the terms of the Creative Commons Attribution License (CC BY). The use, distribution or reproduction in other forums is permitted, provided the original author(s) and the copyright owner(s) are credited and that the original publication in this journal is cited, in accordance with accepted academic practice. No use, distribution or reproduction is permitted which does not comply with these terms.